JOC The Journal of Organic Chemistry

Article

pubs.acs.org/joc

Experimental and Computational Mechanistic Investigation of Chlorocarbene Additions to Bridgehead Carbene–Anti-Bredt Systems: Noradamantylcarbene–Adamantene and Adamantylcarbene–Homoadamantene

Stephanie R. Hare,[†] Marina Orman,[‡] Faizunnahar Dewan,[‡] Elizabeth Dalchand,[‡] Camilla Buzard,[‡] Sadia Ahmed,[‡] Julia C. Tolentino,[‡] Ulweena Sethi,[‡] Kelly Terlizzi,[‡] Camille Houferak,[‡] Aliza M. Stein,[‡] Alexandra Stedronsky,[‡] Dasan M. Thamattoor,[§] Dean J. Tantillo,[†] and Dina C. Merrer*[,‡]

[†]Department of Chemistry, University of California—Davis, 1 Shields Avenue, Davis, California 95616, United States

[‡]Department of Chemistry, Barnard College, 3009 Broadway, New York, New York 10027, United States

[§]Department of Chemistry, Colby College, 5750 Mayflower Hill, Waterville, Maine 04901, United States

Supporting Information

ABSTRACT: Cophotolysis of noradamantyldiazirine with the phenanthride precursor of dichlorocarbene or phenylchlorodiazirine in pentane at room temperature produces noradamantylethylenes in 11% yield with slight diastereoselectivity. Cophotolysis of adamantyldiazirine with phenylchlorodiazirine in pentane at room temperature generates adamantylethylenes in 6% yield with no diastereoselectivity. ^{1}H NMR showed the reaction of noradamantyldiazirine + phenylchlorodiazirine to be independent of solvent, and the rate of noradamantyldiazirine consumption correlated with the rate of ethylene formation. Laser flash photolysis showed that reaction of phenylchlorocarbene + adamantene was independent of adamantene concentration. The reaction of phenylchlorocarbene + homoadamantene produces the ethylene products with $k = 9.6 \times 10^5$ M^{-1} s^{-1}. Calculations at the UB3LYP/6-31+G(d,p) and UM062X/6-31+G(d,p)//UB3LYP/6-31+G(d,p) levels show the formation of exocyclic ethylenes to proceed (a) on the singlet surface via stepwise addition of phenylchlorocarbene (PhCCl) to bridgehead alkenes adamantene and homoadamantene, respectively, producing an intermediate singlet diradical in each case, or (b) via addition of PhCCl to the diazo analogues of noradamantyl- and adamantyldiazirine. Preliminary direct dynamics calculations on adamantene + PhCCl show a high degree of recrossing (68%), indicative of a flat transition state surface. Overall, 9% of the total trajectories formed noradamantylethylene product, each proceeding via the computed singlet diradical.

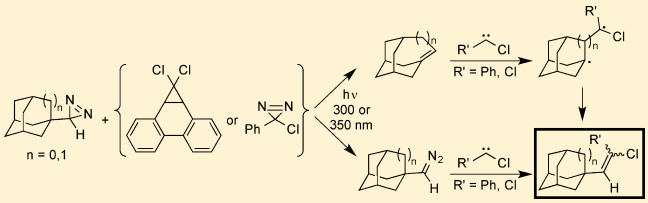

INTRODUCTION

Molecules with strained, distorted geometries fascinate chemists, whether from the sheer challenge of synthesizing these seemingly unfathomable (by the laws of chemistry) structures or simply the beauty of the "abnormal".[1] In particular, the geometries, stabilities, and reactivities of bridgehead alkenes have been a source of intrigue since Bredt proposed his rule almost a century ago.[2−4] Increasing numbers of natural products containing bridgehead alkenes have been isolated and characterized, and their total syntheses achieved.[5] Bridgehead alkenes show diverse reactivity: carbocation rearrangements[6] to Diels–Alder chemistry[7] to radical trapping.[8]

The Jones[7,9−14] and Michl[8,15,16] groups were the among first to study and use bridgehead carbenes as a route to bridgehead alkenes.[17] Among the compounds they studied were adamantene (**3a**)[7−9,15,16] and homoadamantene (**3b**).[11,14−16] The Platz group generated **3a** and **3b** photochemically from noradamantyldiazirine (**1a**) and adamantyldiazirine (**1b**), respectively (Scheme 1).[18,19] The photochemistry of both noradamantyldiazirine (**1a**) and adamantyldiazirine (**1b**) is quite complex. In 2001, Platz and co-workers reported that the photolysis of noradamantyldiazirine (**1a**) leads to adamantene (**3a**) through the excited state of the diazirine, bypassing noradamantylcarbene (**2a**).[18,19] They computed the singlet **2a** ⇌ **3a** equilibrium to greatly favor **3a** by 32.4 kcal/mol (B3LYP/6-31G*) and a nominal 0.35 kcal/mol barrier for the conversion of singlet adamantylcarbene to adamantene.[18]

The minimal barrier for conversion of **2a** → **3a** helped explain Platz and colleagues's matrix isolation and laser flash photolysis (LFP) studies of the photolysis of **1a**. They did not observe **2a** upon photolysis of **1a** at 350 nm in an Ar matrix at 14 K, but they did see UV and IR features attributed to **3a**: UV–vis λ_{max} = 320 nm, IR υ = 1478 cm^{-1}.[19] In benzene[19] or cyclohexane[18] solution, LFP of **1a** produced an absorption assigned to **3a** (λ_{max} = 325 nm) that decayed over "many microseconds" via second-order processes. These processes were attributed to the formation of [2 + 2] dimers of **3a** and

Received: February 27, 2015
Published: April 22, 2015

DOI: 10.1021/acs.joc.5b00456
J. Org. Chem. 2015, 80, 5049−5065

Scheme 1. Irradiation of Diazirines 1 and Their Reactions with PhCCl and CCl_2

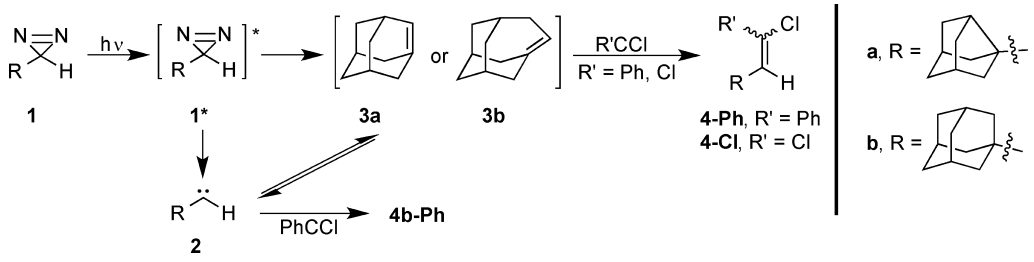

protoadamantene (**5**). Additionally, bimolecular rate constants of the reactions of **3a** with quenchers were determined: 8.4×10^4 M^{-1} s^{-1} (methanol), 1.8×10^5 M^{-1} s^{-1} (1,3-cyclohexadiene), and 1.4×10^7 M^{-1} s^{-1} (acetic acid).[19] Notably, they were not able to visualize **2a** via the pyridine ylide method,[20,21] lending further support to their claim that noradamantylcarbene was either not formed or did not live long enough to be trapped.

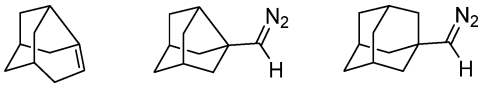

The Platz group also reported the photochemistry of adamantyldiazirine (**1b**).[18] They determined that the minimal structural change of adding one methylene unit in going from **1a** to **1b** resulted in a significant reactivity difference between the two systems. Similar to the noradamantylcarbene–adamantene equilibrium, the computed adamantylcarbene–homoadamantene equilibrium strongly favored homoadamantene: **3b** was 45.9 kcal/mol more stable than singlet **2b** (B3LYP/6-31G*).[18] In contrast to the singlet **2a** → **3a** barrier of 0.35 kcal/mol, the singlet **2b** → **3b** barrier was 6.1 kcal/mol.[18] This increase in the activation barrier indicated that adamantylcarbene may possess a lifetime long enough to be trapped bimolecularly.

Photolysis of **1b** at 350 nm in an Ar matrix at 14 K by Platz and co-workers did not provide UV evidence of **2b**. Rather, **1b** isomerized to adamantyldiazomethane (**6b**; see the structure above). Subsequent photolysis of the **6b**-containing matrix at 254 nm led to the formation of **3b**. LFP of **1b** at 351 nm in pentane or cyclohexane produces no UV-active transient. When pyridine was added, the pyridine ylide of **2b** was produced. The major (stable) products from these photolyses are adducts of **2b** with cyclohexane solvent (11%) and [2 + 2] dimers of homoadamantene, **3b** (28%).[18] From these experiments, they deduced the room-temperature lifetime of **2b** to be 1.5 ns in cyclohexane and 2.5 ns in cyclohexane-d_{12}. They also were able to trap **2b** with piperidine: photolyses in cyclohexane containing increasing concentrations of piperidine resulted in increased **2b**–piperidine adduct and reduced amounts of homoadamantene (**3b**) dimers and **2b**–cyclohexane adducts.[18]

Thus, Platz et al. concluded that the reactive species in the solution-phase chemistry of noradamantyldiazirine was adamantene (**3a**), whereas the reactive species in the solution-phase chemistry of adamantyldiazirine was adamantylcarbene (**2b**).

We are interested in the mechanisms of halocarbene additions to strained C–C π-bonds. Pioneering work by Brinker and co-workers on halocarbene additions to 1,2-diarylcyclopropenes showed evidence of a polar transition state that resulted in the unexpected formation of a butadiene product.[22,23] Brinker's studies stimulated our interest in halocarbene additions to these and similarly strained systems. We since have determined that dihalocarbenes add to cyclopropene and benzocyclopropene in a concerted manner through one transition state that undergoes branching to several products.[24,25] When multiple products are formed from the same transition state, transition state theory is inadequate to describe the reaction mechanism. Rather, nonstatistical dynamic effects may influence or control the course of the reaction. Our dynamics trajectory calculations have strongly supported this phenomenon for dichlorocarbene addition to cyclopropene.[26] We have thus proposed that dynamic effects intervene in carbene additions to π-substrates containing a threshold amount of strain energy. Additionally, Rablen et al. have proposed that reaction dynamics contributes to the regioselectivity of singlet carbene additions to the strained C–C σ-systems of substituted bicyclo[1.1.0]butanes.[27]

In an attempt to determine the threshold strain energy required for dynamics to exert control of carbene addition reactions to strained C–C π-substrates, we have investigated the photochemical reactions of R′CCl (R′ = Ph, Cl) with bridgehead alkenes adamantene (**3a**; E_{strain} = 37–40 kcal/mol) and homoadamantene (**3b**; $E_{strain} \approx 20$ kcal/mol).[11,28] We first desired to determine if these reactions of two transient species (PhCCl + **3a** and PhCCl + **3b**) would yield product at all, given the highly reactive nature of all involved species. Once PhCCl adducts of each system were indeed produced, we used additional experimental (NMR, LFP) and computational tools to make sense of their formation. We thus report the first trapping of transient bridgehead alkenes with carbenes and that these reactions proceed in a stepwise manner via a diradical on the singlet reactive surface of each system or via an S_N2 reaction with the diazo analogues of noradamantyldiazirine and adamantyldiazirine, **6a** and **6b**, respectively.

RESULTS AND DISCUSSION

Product Studies. We synthesized diazirines **1**[18,19,29] and cophotolyzed each with phenylchlorodiazirine (**8**)[30] at 350 nm at room temperature in pentane; **1a** was also cophotolyzed with the phenanthride precursor of CCl_2 (**7**),[31–33] at 300 nm. Products corresponding to the addition of **2a** or **3a** plus each of chlorocarbenes R′CCl and products corresponding to the addition of **2b** or **3b** plus PhCCl were isolated and purified. NMR (^{1}H, ^{13}C, DEPT-135, HSQC, HMBC, NOESY) and HRMS characterization reveal these products to have structures corresponding to **4a-Ph** and **4a-Cl**, and **4b-Ph**, respectively. As determined by GC, the photosylate of **1a** + **8** contains 11% of **4a-Ph**, **1a** + **7** gives 5% of **4a-Cl**, and **1b** + **8** yields 6% of **4b-Ph**. Additionally, the formation of **4a-Ph** showed slight diastereoselectivity favoring the *E*-isomer: the *E*:*Z* ratio was 58.2 ± 0.7:41.8 ± 0.7. There was no preference for either

DOI: 10.1021/acs.joc.5b00456
J. Org. Chem. 2015, 80, 5049–5065

Scheme 2. Proposed Mechanisms of the Formation of Alkene 4a from Cophotolysis of 1a with 7 or 8

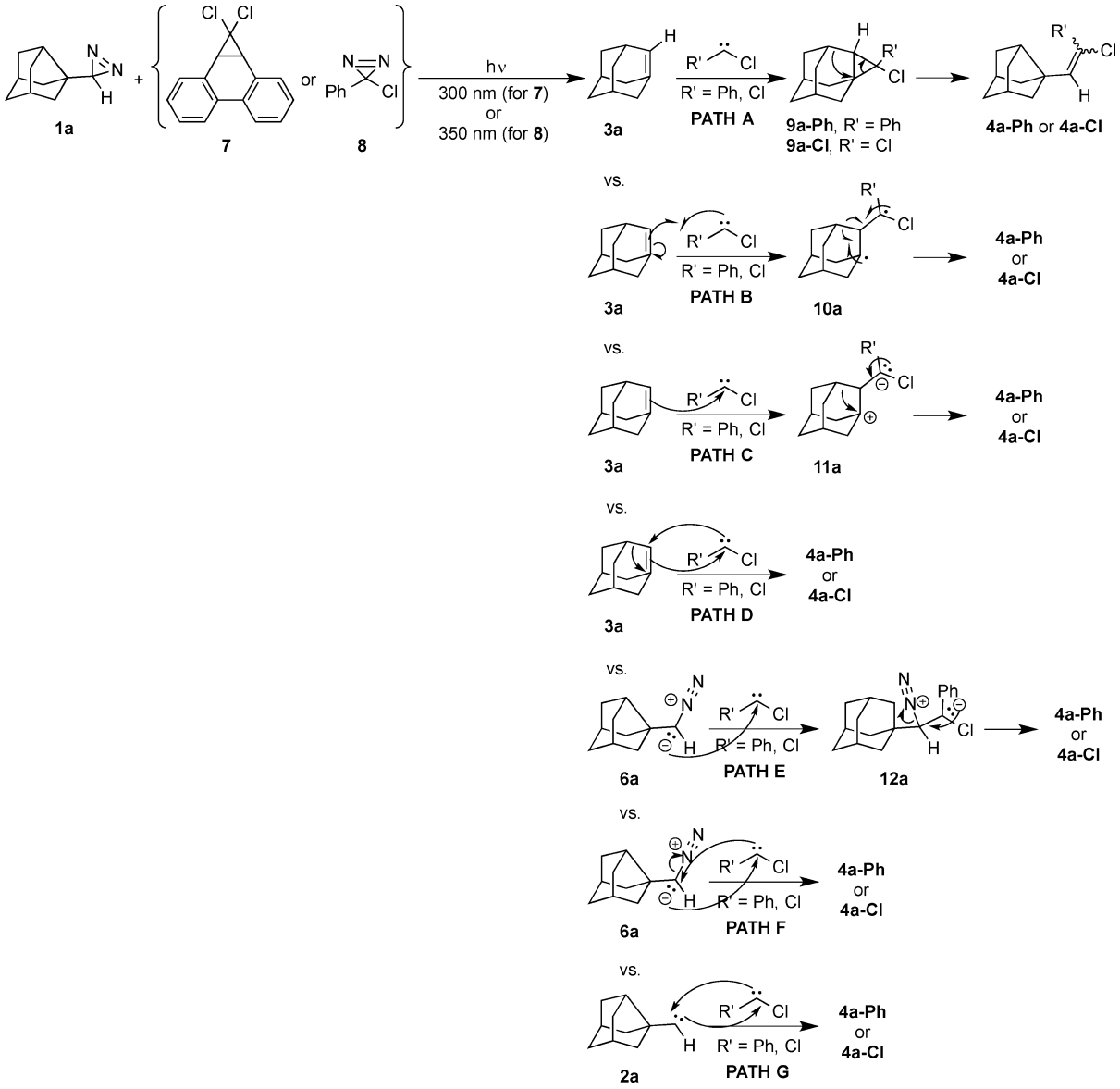

diastereomer of **4b-Ph**: the *E*:*Z* ratio was 48.4 ± 2.1:51.6 ± 2.1. The majority of the remainder of the photosylates are comprised of reactions of PhCCl with pentane, PhCCl dimerization, adamantene dimerization (which had also been reported by Platz),[18,19] homoadamantene dimerization (which also had been reported by Platz),[18] and adducts of each of noradamantylcarbene/adamantene + pentane and adamantylcarbene/homoadamantene + pentane. A table containing the product distributions is included in the Supporting Information. Although the yields were low, the formations of **4a** and **4b** were the most important and the most unanticipated. We not only were surprised by their formation at all, as a result of the reaction of two transients, we were surprised by their structures. We discuss possible mechanisms and our experimental and computational investigations of these possibilities below.

Possible Mechanisms of Formation of Exocyclic Alkenes 4. *Noradamantyldiazirine/Adamantene System.* Scheme 2 depicts several proposed mechanisms for the formation of noradamantylethylene **4a**. The first four pathways center on PhCCl reacting with adamantene **3a**. Path A involves PhCCl cycloaddition to **3a** followed by ring contraction via cyclopropane intermediate **9a**. In paths B and C, R′CCl adds to **3a** in a stepwise manner via a diradical (path B) or zwitterion (path C) followed by concurrent ring contraction and rearrangement to **4a**. These proposed stepwise paths are rooted in evidence provided by Brinker's group of a polar transition state, if not a full zwitterionic intermediate, and the stepwise character of dihalocarbene additions to 1,2-diarylcyclopropenes,[22,23] as well as the involvement of a zwitterion—and thus a nonconcerted pathway—in singlet carbene addition to bicyclo[1.1.0]butanes proposed by Rablen et al.[27] Path D depicts the possibility of the concerted addition and ring contraction of R′CCl + **3a** → **4a**. Path D has a lot of concurrent motion and may seem unconventional, but it is not unfounded, as it parallels the route by which CCl_2 adds to cyclopropene to produce a 1,1-dichloro-1,3-butadiene (Scheme 4). We previously showed the formation of butadiene to result from dynamic effects.[25,26]

Paths E and F stem from the possible isomerization of **1a** to diazo compound **6a**. Platz and co-workers observed the

DOI: 10.1021/acs.joc.5b00456
J. Org. Chem. 2015, 80, 5049−5065

Scheme 3. Proposed Mechanisms of the Formation of Alkene 4b-Ph from Cophotolysis of 1b with 8

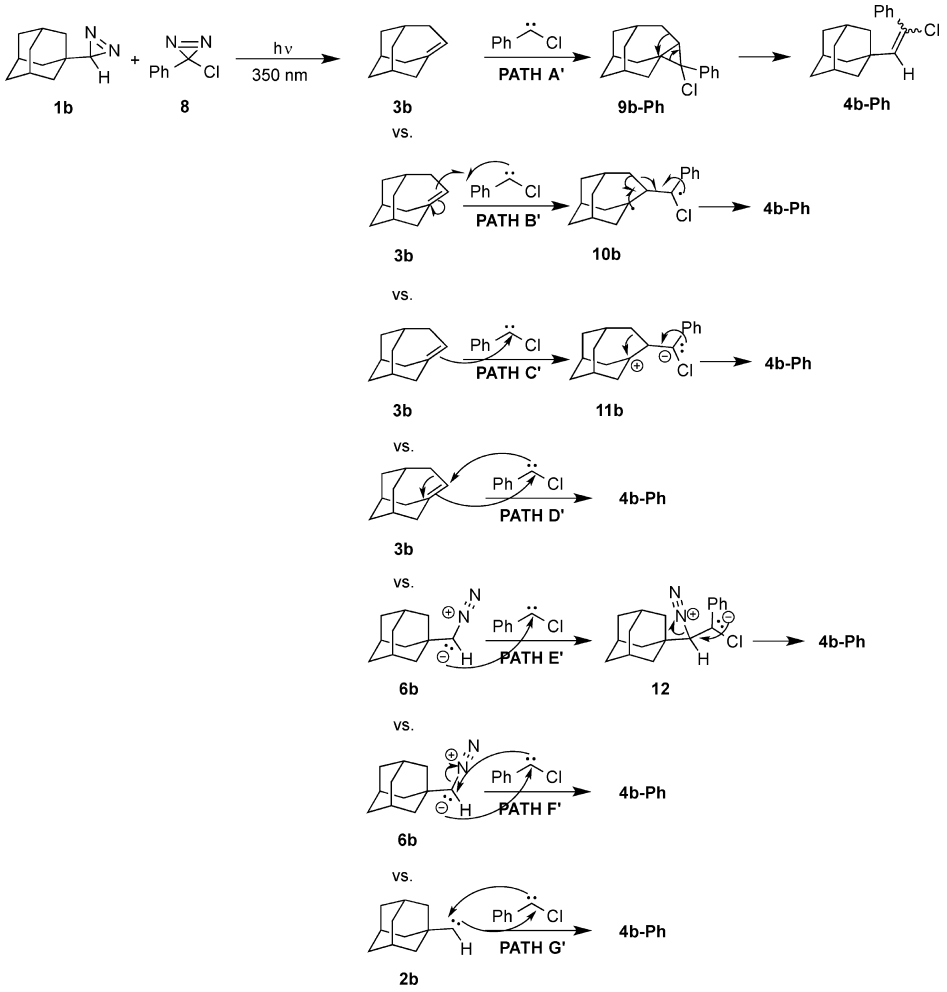

Scheme 4. Mechanism of Formation of Butadiene from CCl_2 Addition to 1,2-Disubstituted Cyclopropenes

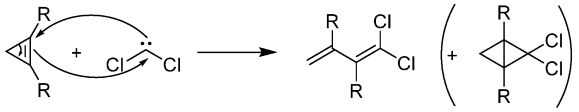

isomerization of **1a** to **6a** in an Ar matrix.[19] Path E outlines stepwise carbene addition to **6a** followed by rearrangement and loss of N_2, whereas path F is the concerted analogue. Lastly, path G forms **4a** via a carbene "dimerization" of R′CCl with noradamantylcarbene (**2a**).

Adamantyldiazirine/Adamantylcarbene System. Given the Platz group's observations of differing photochemistry between noradamantyldiazirine versus adamantyldiazirine, we were surprised by the formation of exocyclic alkenes **4b-Ph** from the cophotolysis of adamantyldiazirine **1b** and phenylchlorodiazirine **8** that paralleled the alkenes obtained from the noradamantyl system (i.e., **4a**). In Scheme 3, we propose mechanisms A′−G′ for the formation of **4b-Ph** analogous to those proposed for the formation of **4a-Ph**. We note that paths E′ and F′ stem from Platz and co-worker's observation of the isomerization of **1b** to diazo compound **6b** in an Ar matrix.[18] Furthermore, the carbene "dimerization" shown in path G′ is the route most consistent with the Platz group's solution-phase photochemical studies of adamantyldiazirine, where adamantylcarbene **2b** was found to be the important reactive intermediate.[18]

Experimental Investigations of Mechanistic Pathways. Because of the ease in obtaining and handling phenylchlorodiazirine (**8**), we focused our experimental and computational mechanistic investigations on the reactions of PhCCl additions to each of the two anti-Bredt systems. These studies are described below.

Noradamantyldiazirine/Adamantene System. To investigate path A experimentally, we monitored the 350-nm photolysis of **1a** + **8** in cyclohexane-d_{12} (C_6D_{12}) and in benzene-d_6 (C_6D_6) at room temperature by UV−vis and ^{1}H NMR spectroscopy, taking spectra at t = 0, 5, 10, 15, 20, 30, 40, and 60 min (three to six trials). The disappearance of **1a** was monitored by following the decay of the diazirine $n \rightarrow \pi^*$ absorption at 340−360 nm (λ_{max} = 358 nm). The starting photolytic solutions in C_6D_{12} and C_6D_6 contained **1a** (ε_{1a} = 330 M^{-1} cm^{-1}) with A_{338} = 1.3−1.4 and **8** (ε_8 = 100 M^{-1} cm^{-1}) with A_{371} = 0.8−0.9. Using ^{1}H NMR, we followed the disappearance of the diazirine proton of **1a** (at δ 0.96 ppm in C_6D_{12} and at δ 0.51 ppm in C_6D_6) and the appearance of the vinyl protons of *E*- and *Z*-**4a-Ph** (at δ 6.43 and 6.52 ppm, respectively, in C_6D_{12}, and at δ 6.29 and 6.33 ppm, respectively, in C_6D_6). The integrations of these protons were calibrated against an internal standard of 0.31 mmol of CH_2Cl_2 in each NMR sample and converted to millimoles of **1a** and to millimoles of *E*- and *Z*-**4a-Ph**.

DOI: 10.1021/acs.joc.5b00456
J. Org. Chem. 2015, 80, 5049−5065

Given the Platz group's report of a tens-of-microseconds lifetime of adamantene at room temperature,[18] we did not expect to see **3a** by NMR, but we did investigate the possibility of the formation (and subsequent disappearance) of cyclopropyl adduct **9a-Ph**. Careful exploration of the far upfield range (δ −0.1 to +0.5 ppm, i.e., where we would expect to observe a cyclopropyl proton resonance) showed no appearance of the putative cyclopropyl proton of **9a-Ph**. Despite our inability to observe **9a-Ph** by NMR, it is entirely possible that **9a-Ph** may form and react faster than can be measured on the NMR time scale.

Although our NMR studies proved inconclusive on the formation of **9a-Ph** in the cophotolysis of **1a** + **8**, we were able to obtain other information about the rates of consumption of diazirine **1a** and production of *E*- and *Z*-**4a-Ph**. Via UV−vis and NMR, we determined that **1a** was consumed by t = 60 min in C_6D_{12} and 40 min C_6D_6. A plot of the millimoles of diazirine **1a** (via integration of the **1a** diazirine proton at δ 0.96 ppm in C_6D_{12} and at δ 0.51 ppm in C_6D_6) versus time showed exponential decay, with $k_{avg} = (1.0 \pm 0.7) \times 10^{-3}$ mmol^{-1} s^{-1} in C_6D_{12} and $1.24 \pm 0.04 \times 10^{-3}$ mmol^{-1} s^{-1} in C_6D_6 (see Supporting Information for graphs). Within 5 min of photolysis, the formation of both *E*- and *Z*-**4a-Ph** was observed by ^{1}H NMR. Although our product studies (see above) exhibited slight diastereoselectivity, we did not measure any significant stereoisomeric preference via these NMR measurements: both diastereomers were produced in equal or nearly equal quantities for the entire 60 min photoreaction. The rate of formation of the two alkenes was determined by summing the integrations of the vinyl protons. By t = 15−20 min in both solvents, generation of **4a-Ph** had maximized and plateaued. A plot of the millimoles of ethylenes **4a-Ph** (via integration of the *E*- and *Z*-**4a-Ph** vinyl protons at δ 6.43 and 6.52 ppm in C_6D_{12} and at δ 6.29 and 6.33 ppm in C_6D_6) versus time showed exponential growth, with $k_{avg} = (2.5 \pm 0.5) \times 10^{-3}$ mmol^{-1} s^{-1} (C_6D_{12}) and $(3.4 \pm 0.8) \times 10^{-3}$ mmol^{-1} s^{-1} (C_6D_6) (see the Supporting Information for graphs). Thus, the rates of disappearance of **1a** and the rates of appearance of **4a-Ph** were each independent of solvent. Additionally, the rate of disappearance of **1a** and the rate of appearance of **4a-Ph** were approximately equal.

Further mechanistic investigation of this system has involved nanosecond kinetics measurements via laser flash photolysis (LFP). We thought that rate constant information would provide additional mechanistic information. In particular, the temperature independence of the bimolecular rate constants for the noradamantyldiazirine + phenylchlorodiazirine system (i.e., **1a** + **8**) would lend support to dynamic control. Additionally, we endeavored to probe whether or not there existed an isotope effect on k_{obs} for **1a** + **8** by measuring the kinetics of the reactions with **1a** and, separately, **1a-*d***.

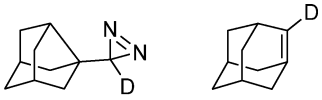

1a-*d* **3a-*d***

As is described below, the isotope effect studies never came to fruition because the consumption of PhCCl was independent of the concentration of parent **2a** or **3a** (via variance of the concentration of **1a**). Hence, we were not able to measure a rate constant for the formation of **4a-Ph** via PhCCl + **2a** or **3a**.

Nevertheless, to obtain rate data for the photolysis of **1a** + **8** at room temperature, we wished to either follow the decay of PhCCl or **3a** (or **3a-*d***) directly; however, these two transients absorb at nearly the same wavelength (λ_{max} = 320 nm for PhCCl and 325 nm for **3a**).[18,19] In need of a clear spectral window, we thus measured the rate of formation of the pyridine ylide[20,21] of PhCCl at 460 nm at varying concentrations of **3a**. To vary the concentration of **3a**, we measured k_{obs} at different concentrations of **1a**. To connect the concentration of **3a** with that of **1a**, separately we measured the A_{325} of **3a** at each concentration of **1a**. The concentration of **1a** ranged from 0.525 to 3.6 mM. Using the reported molar absorptivities of anti-Bredt olefins **13**[34] as an estimate of ε for **3a**, we used Beer's law to obtain the concentration of **3a**. We found k_{obs} for the formation of the pyridine ylide of PhCCl in the presence of **3a** (from **1a**) to be independent of the concentrations of **3a**: k_{obs} = $(4-5) \times 10^7$ M^{-1} s^{-1}. Because the proposed product of **3a** + PhCCl, i.e., **4a-Ph**, is produced in 11% yield (by GC), we conclude that this reaction is not competitive with other processes present in the reaction mixture (e.g., adamantene dimerization, PhCCl insertion into pentane solvent, adamantene or noradamantylcarbene reaction with pentane solvent) to affect k_{obs}.

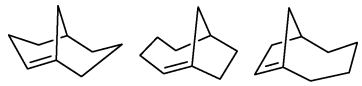

13a **13b** **13c**

Adamantyldiazirine/Adamantylcarbene System. LFP was also used to determine the rate constant for the formation of adamantylethylenes **4b-Ph**, which we believe are formed by the reaction of homoadamantene (**3b**) with PhCCl. The measurements for this system were more straightforward than those for adamantene because homoadamantene does not absorb near PhCCl (λ_{max} of PhCCl = 320 nm).[18] We measured the k_{obs} of the decay of PhCCl at a constant concentration of **1b** at room temperature in pentane: 1.6×10^7 M^{-1} s^{-1}. For these experiments, we make the assumption that a constant concentration of **1b** corresponds to a constant concentration of **3b**. Partitioning k_{obs} according to the product distribution, where **4b-Ph** accounts for 6% of the photolysis products, gives the bimolecular rate constant of 9.6×10^5 M^{-1} s^{-1}. We believe this value to possibly be the first reported rate constant for the reaction of a carbene with homoadamantene.

Computational Investigations of Mechanistic Pathways. Gaussian 09[35] was used to compute the potential energy surfaces (PESs) of several of the proposed mechanisms for the formation of noradamantylethylenes **4a-Ph** and adamantylethylenes **4b-Ph** at the UB3LYP/6-31+G(d,p), UM062X/6-31+G(d,p)//UB3LYP/6-31+G(d,p), and RB3LYP/6-31+G-(d,p) levels of theory (see Computational Methods for details). The energies reported are unscaled, and electronic energies do not include zero-point corrections. All energies are relative to the starting point of carbene **2a** (or **2b**) + PhCCl at infinite separation (E_{rel} or G_{rel} = 0 kcal/mol). Two viable pathways for the formation of **4a-Ph** and **4b-Ph** were found: one that includes the respective anti-Bredt alkene (**3a** or **3b**) and one that does not. We will begin by discussing the pathway on the PESs that includes **3a** or **3b**.

These reactions were computed on the singlet and triplet electronic surfaces. Although the singlet−triplet gap of PhCCl has not yet been determined experimentally, a previous computational study supports a singlet ground state and

DOI: 10.1021/acs.joc.5b00456
J. Org. Chem. 2015, 80, 5049−5065

experimental reactivity from the singlet manifold.[33] We found singlet PhCCl to be 5.4 kcal/mol lower in energy (ΔG) than its triplet state (UB3LYP/6-31+G(d,p) structures in Figure 1),

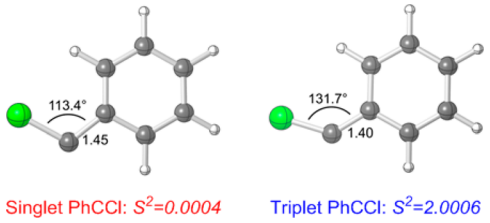

Figure 1. A geometrical comparison of ^{1}PhCCl and ^{3}PhCCl calculated at the UB3LYP/6-31+G(d,p) level of theory. The geometries described here are consistent with previous computations done by the Platz group, who found at the B3LYP/6-31G(d) level of theory the singlet Cl−C−C angle to be 111.8° and the triplet angle to be 131.6°. They also found the C−C bond lengths indicated to be 1.46 and 1.40 Å for the singlet and triplet structures, respectively.[36]

qualitatively consistent with previous computational studies that used several different levels of theory.[36] At this same level of theory and basis set, the triplet state of noradamantylcarbene (**2a**) was 1.1 kcal/mol lower in energy than its singlet state, and triplet adamantylcarbene (**2b**) was the ground state by 0.74 kcal/mol. These nominal differences may be an artifact of the B3LYP functional, which is known to do a poor job of calculating singlet−triplet gaps.[37] For a benchmark study of how this level of theory compares to some experimental singlet−triplet gaps, see the Supporting Information. In any case, the two possible electronic ground states of **2a** and **2b** are likely very close in energy; a pathway involving either electronic state is reasonable.

Noradamantyldiazirine/Adamantene System. We found the lowest energy pathway for the addition of PhCCl to noradamantylcarbene/adamantene to correspond to proposed mechanistic path B (Scheme 2). Previously, the mechanisms of singlet carbene additions to strained C−C π-bonds (cyclopropenes)[22,23] and σ-bonds (bicyclo[1.1.0]butanes)[27] have shown evidence of stepwise character, albeit via polar transition states or intermediates. Here, path B, which proceeds on the singlet electronic state surface, was found using UB3LYP/6-31+G(d,p) and UM062X/6-31+G(d,p)//UB3LYP/6-31+G(d,p) and is depicted in Figure 2. In the first step, carbene **2a** undergoes a ring expansion with a nominal barrier of 0.60 kcal/mol to afford adamantene (**3a**), an exothermic transformation which releases 29.9 kcal/mol. This result is consistent with the Platz group's computational findings of the singlet **2a** ⇌ **3a** equilibrium favoring **3a** by 32.4 kcal/mol (B3LYP/6-31G*)

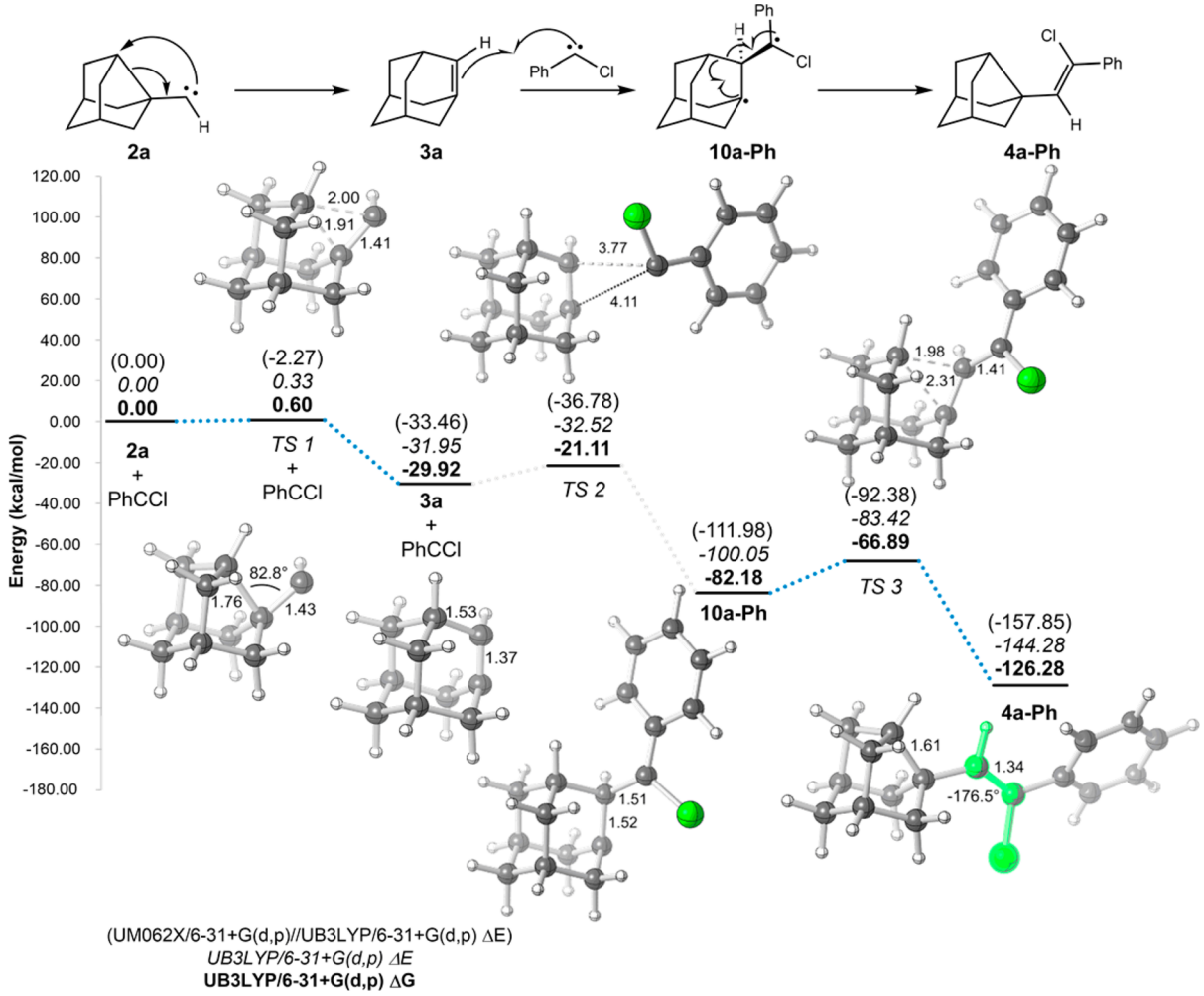

Figure 2. PES of PhCCl addition to noradamantylcarbene (**2a**) and adamantene (**3a**) on the singlet surface at UB3LYP/6-31+G(d,p) (electronic energies E and free energies G) and UM062X/6-31+G(d,p)//UB3LYP/6-31+G(d,p) (electronic energies E).

DOI: 10.1021/acs.joc.5b00456
J. Org. Chem. 2015, 80, 5049−5065

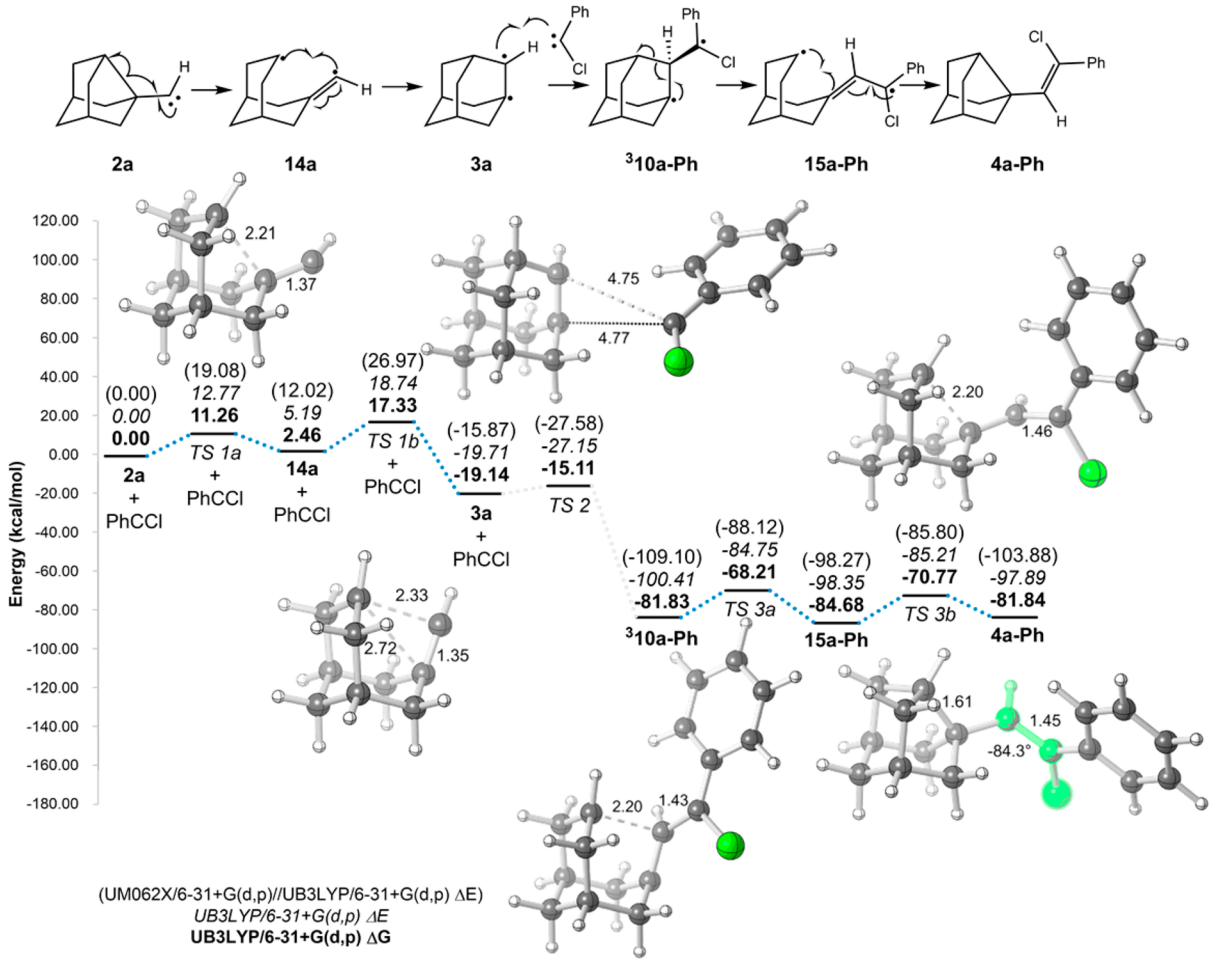

Figure 3. PES of PhCCl addition to noradamantylcarbene (**2a**) and adamantene (**3a**) on the triplet surface at UB3LYP/6-31+G(d,p) (electronic energies *E* and free energies *G*) and UM062X/6-31+G(d,p)//UB3LYP/6-31+G(d,p) (electronic energies *E*). Images of stationary point structures other than TSSs and triplet **4a-Ph** are omitted for clarity (see the Supporting Information).

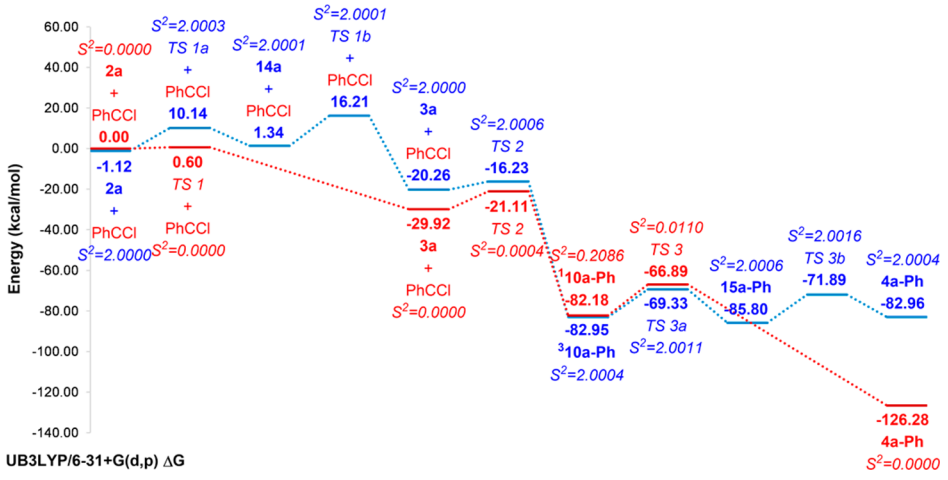

Figure 4. Comparison of singlet (red) and triplet (blue) free-energy PESs of PhCCl addition to noradamantylcarbene (**2a**) and adamantene (**3a**) at UB3LYP/6-31+G(d,p), with S^2 values reported for each stationary point.

with a 0.35 kcal/mol barrier for the conversion of singlet **2a** to **3a**.[18] PhCCl then adds to the bridgehead alkene of **3a**, creating diradical **10a-Ph** in another extremely exothermic step, releasing 52.3 kcal/mol. The final transition-state structure (TSS) corresponding to ring contraction and rearrangement of the adamantyl moiety to **4a-Ph** must overcome a barrier of 15.3 kcal/mol via *TS 3* before 44.1 kcal/mol is released in this step.

A complicating factor of this pathway is that *TS 2*, the TSS corresponding to the addition of PhCCl to adamantene (**3a**), is an extremely early transition state. The distance between the atoms of the forming bond (the carbene carbon of PhCCl and

DOI: 10.1021/acs.joc.5b00456
J. Org. Chem. 2015, 80, 5049−5065

the nonbridgehead alkene carbon of **3a**) is 3.77 Å in *TS 2*. The free energy of activation for this step is 8.8 kcal/mol, where this value is dominated by the entropy penalty of bringing the two molecules together. The electronic energy of *TS 2* including zero point energy corrections is a nominal 0.41 kcal/mol *lower* than that of **3a** + PhCCl at infinite separation, implying that the addition is electronically barrierless. Unfortunately, an intrinsic reaction coordinate (IRC) connecting *TS 2* to either of its flanking minima (**3a** + PhCCl or **10a-Ph**) could not be found. We infer that this difficulty stems from the flatness of the PES around **3a** + PhCCl, making the minimum energy path difficult to elucidate.

While only the pathway corresponding to *Z*-**4a-Ph** is illustrated above, both *E*- and *Z*-isomers were observed experimentally, with slight preference for the *E*-diastereomer: *E*:*Z* = 1.4. It is postulated that the product's alkene geometry is defined in *TS 3*, because free rotation around the newly formed single C−C bond of **10a-Ph** would allow either isomer to form (in the absence of nonstatistical dynamic effects). Compared to the 15.3 kcal/mol barrier that precedes formation of *Z*-**4a-Ph**, the *TS 3* structure corresponding to formation of *E*-**4a-Ph** exhibited a free energy barrier of 17.4 kcal/mol. A $\Delta\Delta G$ of 2 kcal/mol would mean almost exclusive experimental formation of the product with the lower-energy TSS, and nonstatistical dynamics could be causing the ratio of isomers seen experimentally (vide infra).

The analogous triplet pathway for the same mechanism of noradamantylcarbene/adamantene + PhCCl is shown in Figure 3, and a comparison of the singlet and triplet PESs for this reaction is depicted in Figure 4. Although triplet **2a** (^{3}**2a**) was found to be lower in energy than singlet **2a** (^{1}**2a**), the barrier for rearrangement of ^{1}**2a** to ^{1}**3a** (via *TS 1* in Figure 1) is approximately 10 kcal/mol lower in energy than the first TSS for the rearrangement of ^{3}**2a** to ^{3}**3a** (i.e., *TS 1a* in Figure 3). Because the barrier on the singlet surface is so small, the collapse of ^{1}**2a** to ^{1}**3a** is expected to be rapid at room temperature. The ease of ^{1}**2a** → ^{1}**3a** was invoked by Platz and co-workers as the reason why adamantene served as the reactive species in their studies and why they were unable to detect the formation of noradamantylcarbene.[18] The singlet pathway is calculated to be the lower-energy path until intermediate **10a-Ph**, where the triplet structure of this species is 0.77 kcal/mol lower in energy than the singlet. The activation barrier to descend to the next minimum is also slightly lower for the triplet path (via *TS 3a* in Figure 3) than the singlet path (via *TS 3* in Figure 2) by approximately 1.7 kcal/mol. Because intermediate **10a-Ph** is a distal diradical, the radical electrons likely do not interact significantly. This is evidenced by the fact that ^{3}**10a-Ph** and ^{1}**10a-Ph** are very similar in energy and geometry. While it is possible for crossing to occur between the singlet and triplet surfaces in this system, singlet **4a-Ph** is undoubtedly the expected product, being 40 kcal/mol lower in energy than its triplet counterpart.

The triplet version of species **2a** was calculated to be lower in energy than its singlet counterpart by 1.12 kcal/mol. While this energy difference is small and might be an artifact of the level of theory employed, it is also possible that this reaction proceeds through an excited state of **2a**. A map of the spin densities for each stationary point along the transformation from PhCCl adding to **3a** to the final alkene product is shown in Figure 5. These surfaces show how unpaired spin density evolves along the reaction coordinate. Of particular note is the spin density for **10a-Ph**, which shows separate alkyl and benzyl radical

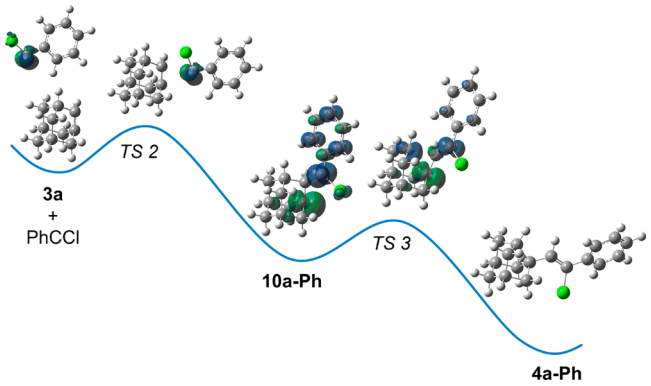

Figure 5. Spin density map of the transformation from separate species **3a** and PhCCl to alkene product, **4a-Ph** [isovalue = 0.005; UB3LYP/6-31+G(d,p)].

subsystems. In the preceding TSS, *TS 2*, the unpaired spin density is localized on the attacking carbene fragment, consistent with how early this TSS is, and the alkene fragment does not display diradical character, despite its distorted geometry. In the subsequent TSS, *TS 3*, the spin density shifts away from the aromatic ring and onto carbon atoms involved in the alkyl shift.

The other mechanistic possibilities in Scheme 2 were investigated with limited success. A TSS corresponding to a concerted addition of PhCCl to **3a** to afford cyclopropane **9a-Ph**, as illustrated in path A of Scheme 2, could not be found, perhaps due to the twist of the C=C π-bond in **3a** (see below). Additionally, attempts at finding a TSS for the rearrangement of **9a-Ph** to the alkene product **4a-Ph** only afforded a TSS corresponding to cyclopentene product **16a-Ph**, a product observed in the preliminary dynamics studies discussed below and illustrated in Figure 7 but not observed experimentally. Path C was the first complete pathway that was identified when calculations were run using RB3LYP/6-31+G(d,p). However, when the pathway was calculated using the same level of theory, but using an unrestricted wave function to allow the possibility of unpaired electrons, diradical **10a-Ph** was found to be lower in free energy than zwitterion **11a-Ph** by 16.6 kcal/mol. No TSS corresponding to path D, in which **3a** ring-opening and PhCCl addition occurs in a single concerted step, could be located.

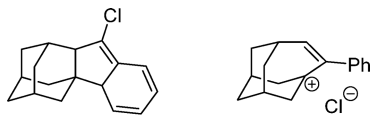

16a-Ph **17a-Ph**

Paths E and F were investigated by attempting to locate a TSS with a tetrahedral carbon center, corresponding to PhCCl addition to **6a**. A relaxed PES scan of the distance between the diazo carbon of **6a** and the carbene carbon of PhCCl from 3.70 to 1.60 Å in steps of 0.15 Å exhibited a distinct maximum at a distance of about 2.20 Å. The structure with this C−C distance was optimized to a TSS, revealing another possible pathway for **4a-Ph** formation (see below). The stepwise version of this pathway, path E, was discounted as **12a-Ph** was not found to be a minimum on the PES at this level of theory.

Path G was investigated using a similar method, with a scan along the distance between carbene carbons of **2a** and PhCCl. The addition appeared to be electronically barrierless and no

DOI: 10.1021/acs.joc.5b00456
J. Org. Chem. 2015, 80, 5049−5065

TSS could be located, but a free energy barrier is expected due to the entropy penalty associated with bringing two carbenes together. It is additionally inferred that the small barrier and high exothermicity in the rearrangement of carbene **2a** to anti-Bredt alkene **3a** mean that the lifetime of **2a** is too short for it to be the reactive species in this bimolecular addition, in accord with the Platz group's findings.[18]

Despite releasing approximately 30 kcal/mol of energy in its formation, the geometry of singlet **3a** has significant strain. Figure 6d illustrates the degree of "twisting" that this alkene exhibits compared to an unstrained olefin, where the C−C−C−C dihedral angle of the alkene is 85.1°, significantly smaller than an unstrained 180° geometry. While the ideal bond angles around an sp^2-hybridized carbon would be 120°, this structure is forced to have only one angle near ideal (119.2°) and the others markedly smaller, closer to an ideal sp^3-hybridized carbon bond angle (Figure 6b,c). Another indication of strain in this molecule is its longer-than-average alkene bond length of 1.37 Å, whereas the average unstrained alkene bond length is closer to 1.33 Å (Figure 6a). See the Supporting Information for a detailed distortion-interaction analysis[38,39] of *TS 2*.

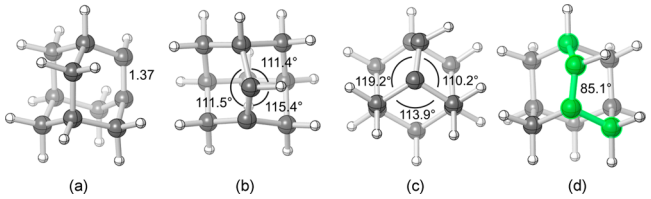

Figure 6. Four views of the geometry of adamantene (**3a**) at UB3LYP/6-31+G(d,p). (a) A side view, with the alkene bond length labeled (in angstroms). (b) A centralized view of the nonbridgehead carbon of the alkene. This carbon is highly pyramidalized, with the sum of the angles labeled being 328.3°. (c) A view of the bridgehead carbon of the alkene. This sp^2-hybridized carbon is also pyramidalized, with the sum of the angles labeled being 343.3°. (d) One of the C−C−C−C dihedral angles of the alkene portion of **3a** is highlighted in green. While this angle in a planar alkene would be closer to 180°, the tricyclic nature of **3a** forces the dihedral into a strained 85.1° configuration. The significant "twist" exhibited by the C−C π-bond prompts its unique reactivity.

Previous studies have shown that carbene additions to strained C−C π-bonds may result in product formation that is controlled by nonstatistical dynamics.[22,23,25,26,40−44] The high exothermicity of each intermediate step in the singlet diradical-mediated mechanism of PhCCl addition to adamantene (i.e., path B) and the relative shallowness of each intermediate well were grounds to begin a preliminary dynamics study. Additionally, because an IRC connecting *TS 2* with **10a-Ph** could not be calculated, dynamics calculations would help substantiate a connection between *TS 2* and the product.

We thus computed direct dynamics trajectories with a time step of 1 fs initiated at singlet *TS 2* for path B using Gaussian 09 at UB3LYP/6-31+G(d,p) (see Computational Methods for details), the results of which are shown in the table embedded in Figure 7. A total of 47 (68%) of 69 trajectories resulted in recrossing, where the separated reactants **3a** and PhCCl (characterized as separated by a distance of 5 Å) formed on either side of the TSS. We know *TS 2* to be a quite early TSS, and these results lend support to the flatness of the PES around *TS 2*, making it more difficult for *TS 2* to evolve toward the descent to **10a-Ph**. This high degree of crossing may also be due to use of the transition state associated with electronic energy rather than a variational transition state. The other 32% of the trajectories proceeded to possible products, with six trajectories (9%) leading to the observed products **4a-Ph**. Though no conclusions about computational (dynamics) versus experimental product ratios from a sample size this

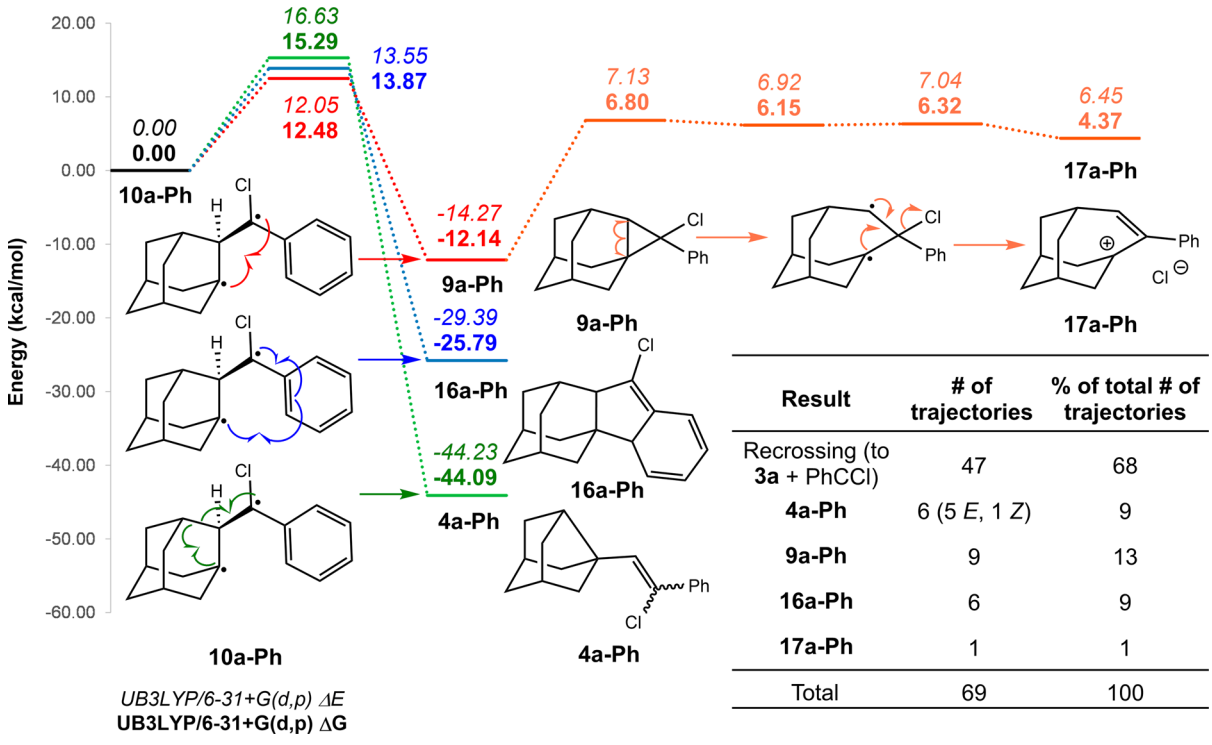

Result	# of trajectories	% of total # of trajectories
Recrossing (to **3a** + PhCCl)	47	68
4a-Ph	6 (5 *E*, 1 *Z*)	9
9a-Ph	9	13
16a-Ph	6	9
17a-Ph	1	1
Total	69	100

Figure 7. Results of direct dynamics calculations of **3a** + PhCCl. Trajectories were initiated at *TS 2* [UB3LYP/6-31+G(d,p)].

DOI: 10.1021/acs.joc.5b00456
J. Org. Chem. 2015, 80, 5049−5065

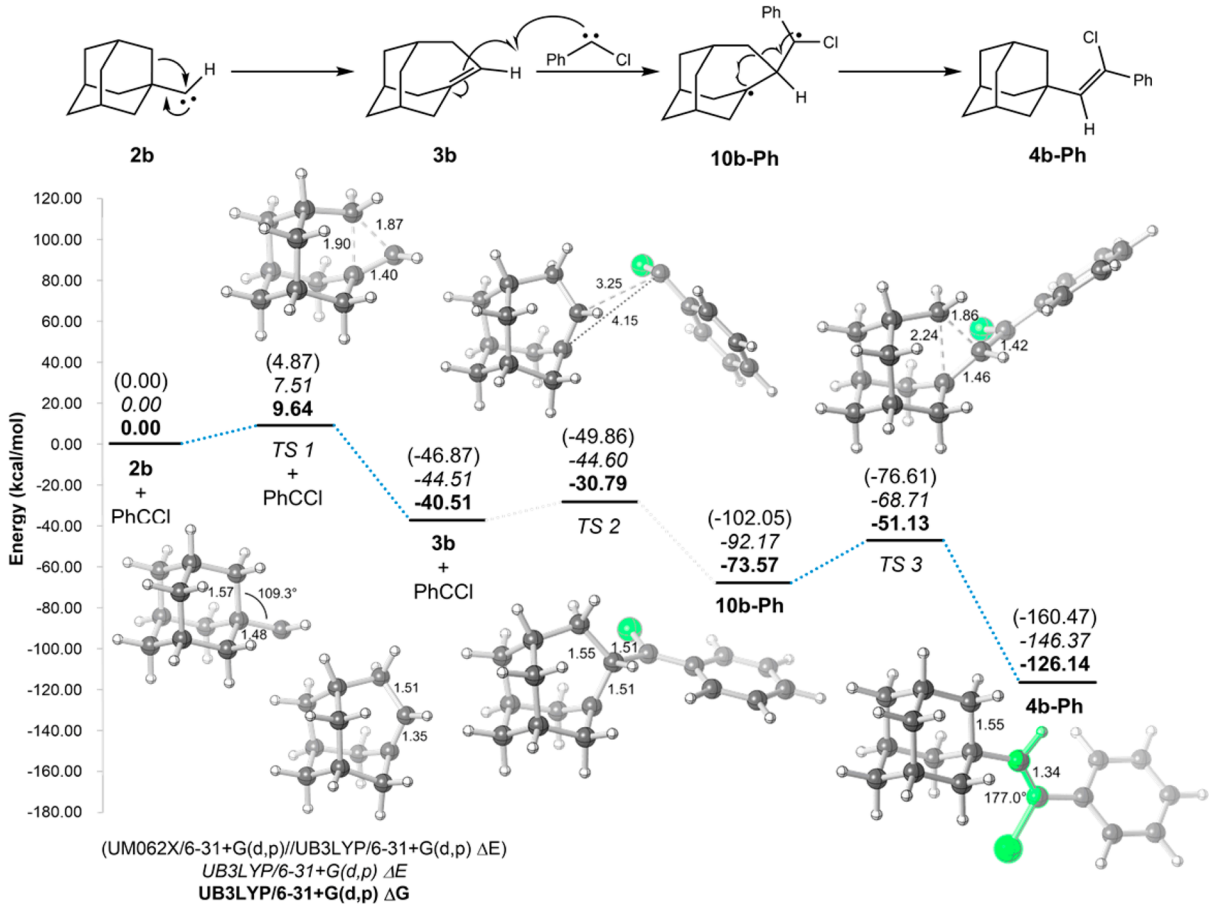

Figure 8. PES of PhCCl addition to adamantylcarbene (**2b**) and homoadamantene (**3b**) on the singlet surface at UB3LYP/6-31+G(d,p) (electronic energies *E* and free energies *G*) and UM062X/6-31+G(d,p)//UB3LYP/6-31+G(d,p) (electronic energies *E*).

small can be drawn, it is of note that both diastereomers of **4a-Ph** were observed in the six dynamics trajectories that led to this product (five *E* and one *Z*). The fact that both isomers formed may be indicative of nonstatistical dynamics playing a role in the ratio of *E*- vs *Z*-isomers obtained experimentally. Another nine trajectories (13%) resulted in the formation of cyclopropane **9a-Ph**. An additional six trajectories (9%) resulted in the formation of a cyclopentene **16a-Ph** that was not observed experimentally, and one trajectory (1%) resulted in chloride dissociation (to **17a-Ph**). Notably, every trajectory that did not result in recrossing, including those forming **9a-Ph**, **16a-Ph**, and **17a-Ph**, proceeded through diradical **10a-Ph**, supporting the proposed mechanism (path B).

The TSSs corresponding to possible ring closing of **10a-Ph** to cyclopropane **9a-Ph** and cyclopentene **16a-Ph** were investigated. Surprisingly, the barrier for **10a-Ph** undergoing ring closure to **9a-Ph** was 12.5 kcal/mol and the barrier for **10a-Ph** → **16a-Ph** was found to be 13.9 kcal/mol, which are both lower than the 15.3 kcal/mol barrier for **10a-Ph** → **4a-Ph**, though neither **9a-Ph** nor **16a-Ph** was observed experimentally. The sample size in this preliminary investigation of the role of dynamics in this reaction is small. A more in-depth dynamics study beyond the scope of the current investigation would need to be undertaken to draw definitive conclusions from the results, but the formation of **9a-Ph** and **16a-Ph** in the dynamics calculations yet not in the experiments, along with the fact that their computed TSSs are low in energy, hints that nonstatistical dynamic effects may play a role in this reaction in a way that is not able to be captured by this small sample of trajectories.

Adamantyldiazirine/Adamantylcarbene System. As shown in Figure 8, the lowest energy route for the addition of PhCCl to adamantylcarbene (**2b**)/homoadamantene (**3b**) is analogous to that for the previous system, i.e., path B′ (Scheme 3) on the singlet surface. The PES shown in Figure 8 was computed at the UB3LYP/6-31+G(d,p) and UM062X/6-31+G(d,p)//UB3LYP/6-31+G(d,p) levels of theory (see Computational Methods for details). Although the overall mechanism parallels that found for noradamantylcarbene/adamantene, there are several key differences. Whereas the barrier to rearrangement of noradamantylcarbene **2a** to adamantene **3a** was <1 kcal/mol, the barrier for rearrangement of adamantylcarbene **2b** to homoadamantene **3b** is a more substantial 9.6 kcal/mol, consistent with the Platz group's previous findings.[18] This barrier height suggests a longer lifetime of carbene **2b**, which is once again supported experimentally by Platz et al.'s LFP studies, which found the reactive species of adamantyldiazirine in solution to be carbene **2b**.[18] The additional barrier for this system can be justified physically by comparing the optimized geometries of singlet **2a** and **2b** (Figure 9). The miniscule rearrangement barrier of **2a** to **3a** is likely a result of σ_{C-C} donation into the empty p-orbital of the carbene. The C−C−C angle between the carbons of the donating C−C bond and the carbene carbon is an acute 82.8°, indicating significant orbital overlap. This donation lengthens, and weakens, the C−C bond to be inserted into, lowering the rearrangement barrier. The

DOI: 10.1021/acs.joc.5b00456
J. Org. Chem. 2015, 80, 5049−5065

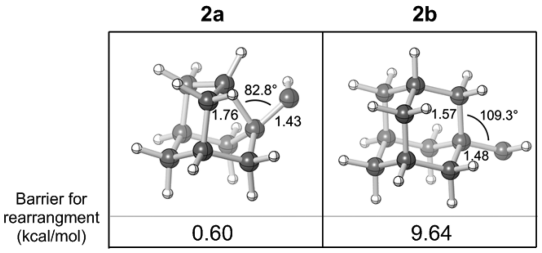

Figure 9. A comparison of the optimized structure geometries of singlet and triplet **2a** and **2b** at UB3LYP/6-31+G(d,p). The rearrangement barrier indicated is that for carbene insertion into a C−C bond to afford **3a** or **3b** in the case of the singlet surfaces or the barrier for the first step of this rearrangement on the triplet suraces. The minimal barrier for rearrangement of ^{1}**2a** to ^{1}**3a** is attributed to σ_{C-C} donation into the empty p-orbital of the carbene.

extra methylene unit of **2b** makes this geometry less favorable, so the bridgehead carbon preferentially adopts tetrahedral bond angles (∼109°).

The rearrangement of **2b** to homoadamantene **3b** releases 40.5 kcal/mol. Singlet PhCCl adds to **3b** in a stepwise manner over a 10.4 kcal/mol barrier (*TS 2*) to give singlet diradical **10b-Ph**. The intermediate well of **10b-Ph** is deeper than that of **10a-Ph**, but the 22.5 kcal/mol barrier to surpass *TS 3* is still possible at room temperature, especially when the formation of **10b-Ph** is calculated to be so exothermic (33.0 kcal/mol released). The final step to form alkene product **4b-Ph** from **10b-Ph** releases 52.6 kcal/mol.

Similar to the noradamantyl system, both diastereomers of **4b-Ph** were seen experimentally and in approximately equal amounts (*E*:*Z* = 0.94). The pathway shown above is that corresponding to formation of *Z*-**4b-Ph**. The *TS 3* structure shown above has a barrier of 22.5 kcal/mol, while that for *E*-**4b-Ph** had a barrier of 25.6 kcal/mol. Again, while this $\Delta\Delta G^{\ddagger}$ of 3.1 kcal/mol would imply that only the *Z*-isomer would be seen experimentally, nonstatistical dynamic effects could be causing both isomers of **10b-Ph** to be formed.

Much like its relative adamantene **3a**, the ground-state singlet structure of homoadamantene **3b** exhibits a twisted geometry (Figure 10). However, the additional methylene in **3b** allows the bridgehead alkene carbon freedom to adopt a more planar geometry than the bridgehead alkene carbon of **3a**. This additional freedom manifests itself in the higher exothermicity of the carbene 1,2-alkyl shift for **2b** → **3b** than for **2a** → **3a**. Additionally, the barrier to PhCCl addition to **3b** is about 1 kcal/mol higher than addition to **3a**, which could be an indication of less strain in olefin **3b**.

As for the noradamantylcarbene/adamantene system, we computed the triplet PES for path B′ (Figure 11). Similar to noradamantylcarbene, although the structure of ^{3}**2b** was calculated to be 0.74 kcal/mol lower in energy than ^{1}**2b**, the barrier for rearrangement of ^{1}**2b** → ^{1}**3b** was 16.1 kcal/mol lower in energy than the first step in the triplet pathway for rearrangement of ^{3}**2b** (to **14b**).

A comparison of the singlet and triplet pathways for the reaction of adamantylcarbene with PhCCl is shown in Figure 12. Once again, the singlet pathway is significantly lower in energy until intermediate **10b-Ph** and *TS 3*, where the singlet and triplet energies are quite close, with the triplet path being slightly lower in energy.

A concerning aspect of the adamantyl triplet pathway is the lack of a barrier when ^{3}**3b** + PhCCl proceeds to *TS 2*. The structure of ^{3}**3b** was optimized separately from PhCCl in order to calculate an approximate energy for that intermediate state. It is possible that ^{3}**3b** + PhCCl may form a loose complex as they are brought together. This putative complex may be lower in energy than *TS 2*, leading to a barrier when surmounting *TS 2*. Calculating the energy of this type of complex was not pursued because we believe the reaction to proceed via the singlet surface, particularly on this part of the PES.

Similar investigations were undertaken for the adamantylcarbene/homoadamantene system as for the noradamantylcarbene/adamantene system to explore other mechanistic possibilities. No TSS for either the concerted addition of PhCCl to **3b** to afford **9a-Ph** or the concerted cyclopropane opening/ring contraction step of path A′ was located. Path C′ was calculated completely, but diradical **10b-Ph** was found to be 24.9 kcal/mol lower in free energy than zwitterion **11b-Ph** (see the Supporting Information). The entirely concerted mechanism in path D′ was discounted when attempts at finding a relevant TSS afforded only the TSS for PhCCl addition to produce **10b-Ph** (Figure 8). A TSS containing a tetrahedral carbon center at the diazo carbon of **6b** was also located for this system, in accordance with path F′ (more below). However, the stepwise analog of this path, path E′, was discounted as intermediate **12b-Ph**, like **12a-Ph**, was not found as a minimum on the PES. A relaxed PES scan along the carbene−carbene distance of PhCCl and **2b** investigated the possibility of path G′. Once again, though the addition appeared electronically barrierless, no TSS was identified for a carbene−carbene mixed dimerization.

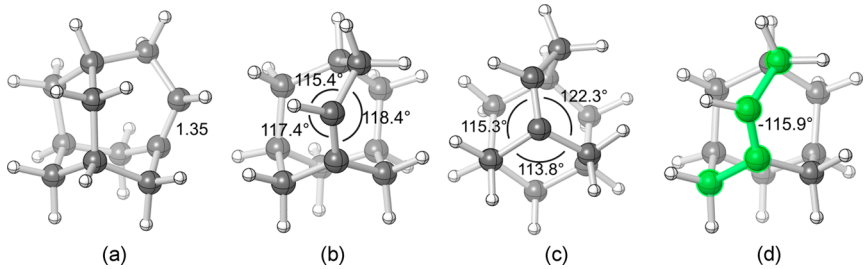

Figure 10. Four views of the geometry of homoadamantene (**3b**) at UB3LYP/6-31+G(d,p). (a) A side view illustrating the alkene bond length (in angstroms). (b) A top view of the nonbridgehead alkene carbon. The sum of the angles labeled is 351.2°. Though not planar, this carbon is significantly less pyramidalized than its analogous carbon in structure **3a** (Figure 6). (c) A top view of the C−C bond angles around the bridgehead carbon. The extra methylene unit of **3b** compared to **3a** allows the bridgehead carbon to be almost planar, demonstrated by the sum of the labeled angles being 351.4°. (d) The −115.9° C−C−C−C dihedral angle highlighted shows there is still noticeable strain in the π-bond, as this value deviates significantly from an ideal −180° dihedral for a planar system.

DOI: 10.1021/acs.joc.5b00456
J. Org. Chem. 2015, 80, 5049−5065

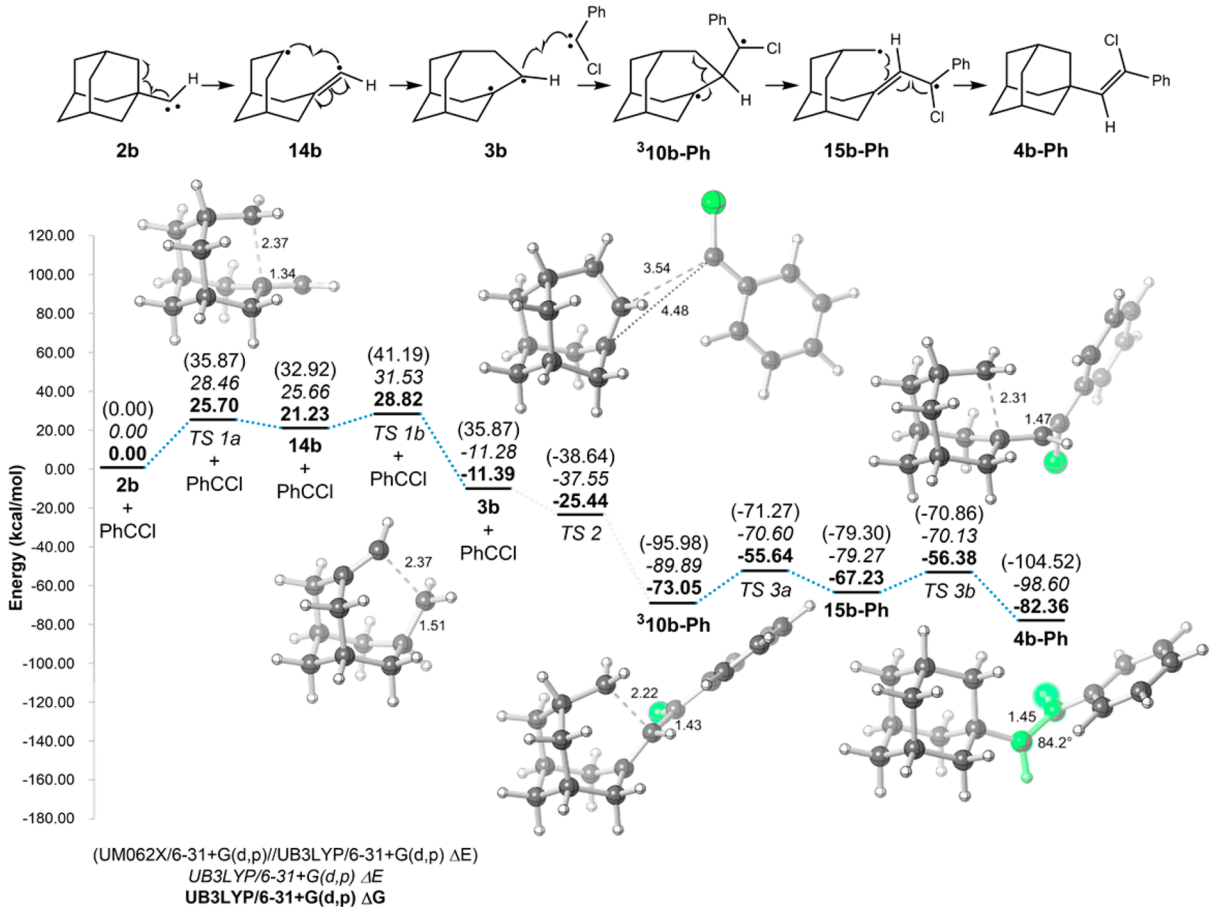

Figure 11. PES of triplet PhCCl addition to adamantylcarbene (**2b**) and homoadamantene (**3b**) on the triplet surface at UB3LYP/6-31+G(d,p) (electronic energies *E* and free energies *G*) and UM062X/6-31+G(d,p)//UB3LYP/6-31+G(d,p) (electronic energies *E*). Images of stationary point structures other than TSSs and triplet **4a-Ph** are omitted for clarity (see the Supporting Information).

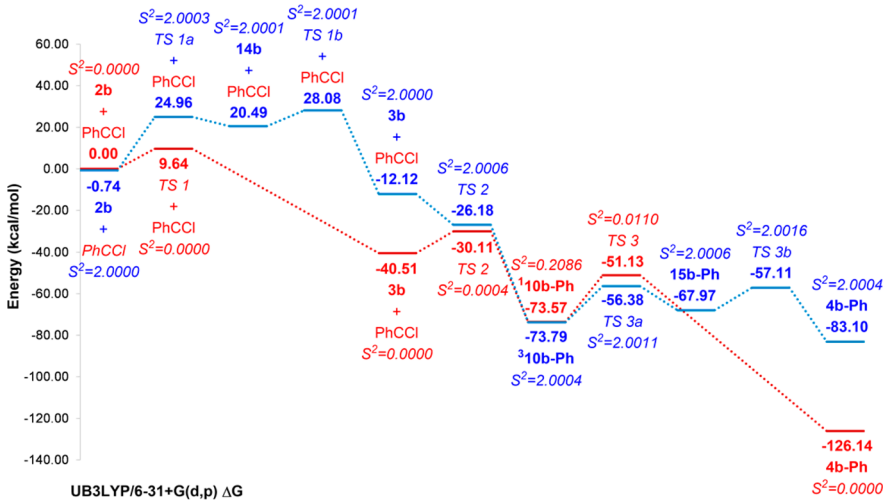

Figure 12. Comparison of singlet (red) and triplet (blue) free-energy PESs of PhCCl addition to adamantylcarbene (**2b**) and homoadamantene (**3b**) at UB3LYP/6-31+G(d,p).

Paths F and F′. The other viable pathway discovered for both systems was path F or F′, in which PhCCl adds to the diazo carbon of **6a** or **6b** in a concerted manner, with N_2 loss occurring without an intermediate. The PESs for paths F and F′ are shown in Figures 13 and 14, respectively.

Path F/F′ is a one-step, S_N2-like mechanism with a barrier of 17.2 kcal/mol in the case of **6a** and a barrier of 17.0 kcal/mol for PhCCl adding to **6b**. In the noradamantyl system, the rate-determining step of path B (*TS 3*) has a barrier of 17.4 kcal/mol for formation of *E*-**4a-Ph**, which, in the absence of other factors, would imply that paths B and F are competitive in formation of the same product. However, this system is complicated by the fact that the two viable pathways found involve two different reactive species: **2a** or **6a**. Rapid

DOI: 10.1021/acs.joc.5b00456
J. Org. Chem. 2015, 80, 5049−5065

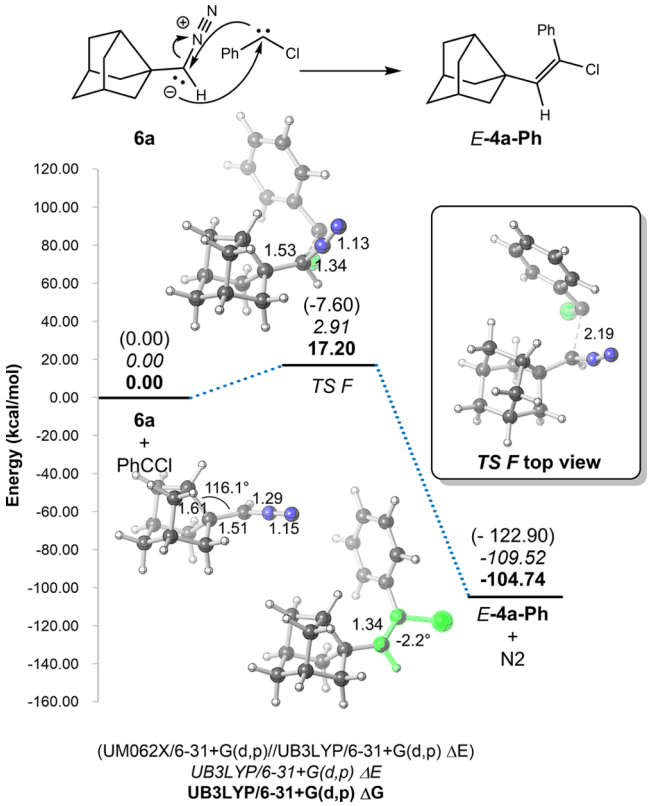

Figure 13. A reaction coordinate diagram of the proposed path F for the noradamantyl system optimized at UB3LYP/6-31+G(d,p) with single point energy calculations at UM062X/6-31+G(d,p)//UB3LYP/6-31+G(d,p).

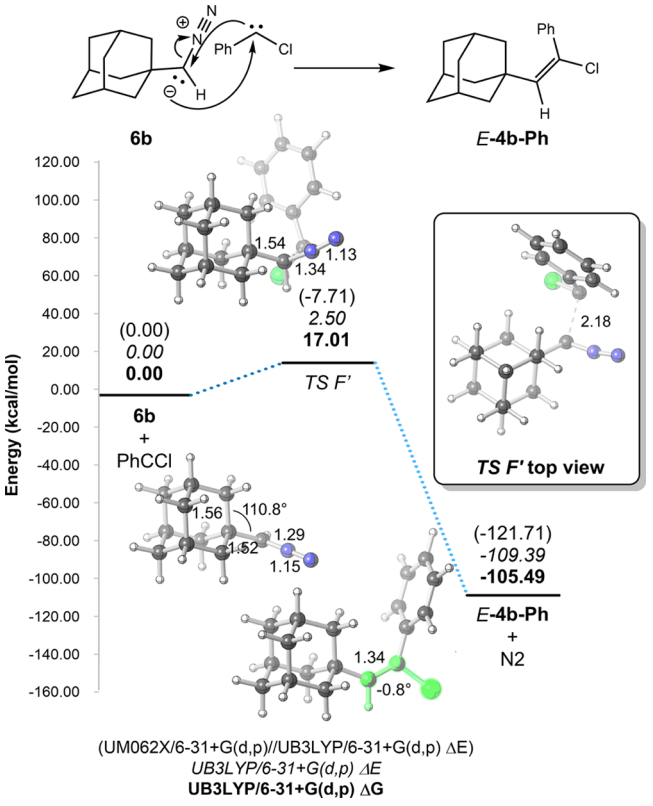

Figure 14. A reaction coordinate diagram of the proposed path F′ for the adamantyl system optimized at UB3LYP/6-31+G(d,p) with single point energy calculations at UM062X/6-31+G(d,p)//UB3LYP/6-31+G(d,p).

interconversion between these two species would need to be assumed in order to say definitively that both of these mechanisms are producing *E*-**4a-Ph**. In the adamantyl system, the rate-determining steps of each path have significantly different barriers. *TS* 3 of path B′ has a barrier of 25.6 kcal/mol, 8.6 kcal/mol greater than the barrier for PhCCl addition to **6b** to afford *E*-**4b-Ph**, which would indicate exclusive formation of product via path F′ if these mechanisms were directly competing.

We are thus left with two mechanistic possibilities: path B/B′ via stepwise addition of PhCCl to bridgehead alkene **3a** or **3b** to yield singlet diradical **10a-Ph** or **10b-Ph** and/or path F/F′ via PhCCl addition to diazo compound **6a** or **6b**. The question remains whether photolysis of **1a** or **1b** at λ = 350 nm at room temperature affords the respective diazo isomer **6a** or **6b**. While the Platz group found the photolysis of noradamantyldiazarine **1a** at λ = 350 nm to produce **3a** via an excited state of **1a**, as well as diazo isomer **6a**, 350 nm irradiation of adamantyldiazirine (**1b**) formed only adamantyldiazomethane **6b**.[18,19]

Because both *E*- and *Z*-**4a-Ph** and **4b-Ph** were observed experimentally, TSSs corresponding to formation of both diastereomers were investigated for paths F and F′. Unfortunately, no TSS for the formation of the *Z*-isomer for either system could be located, leaving us without a clear prediction to compare with the experimental data. It is unclear whether this result is due to physical restrictions on this potential TSS (i.e., it may not be a stationary point on the PES).

In conclusion, it is suspected that the formation of alkene products from the reaction of each of noradamantyl- and adamantyldiazirine with phenylchlorodiazirine proceeds through path B/B′ (singlet diradical) or path F/F′ (diazo addition). While the influence of dynamic control of this reaction is presently unclear, it is possible that the formation of **4-Ph** is controlled by nonstatistical reaction dynamics. A more in-depth dynamics study is necessary to draw definitive conclusions about the role of nonstatistical reaction dynamics in these particular carbene-mediated reactions.

■ CONCLUSIONS

The cophotolysis of noradamantyldiazirine (**1a**) with the phenanthride precursor of dichlorocarbene (**7**) or phenylchlorodiazirine (**8**) produces noradamantylethylenes **4a** in 11% yield. The analogous cophotolysis of adamantyldiazirine **1b** with **8** generates adamantylethylenes **4b-Ph** in 6% yield. Experimentally, the rate of consumption of **1a** was equal to the rate of formation of **4a-Ph**, as determined by ^{1}H NMR. LFP measurements showed PhCCl + adamantene (**3a**) to be independent of the concentration of **3a**, and PhCCl + homoadamantene (**3b**) produces **4b-Ph** with $k = 9.6 \times 10^5$ M^{-1} s^{-1}, which we believe to be the first reported rate constant for the reaction of a carbene with **3b**. Theoretical calculations support the formation of the exocyclic alkene products **4a-Ph** and **4b-Ph** via two possible pathways: (1) stepwise addition of phenylchlorocarbene to adamantene (**3a**) and to homoadamantene (**3b**) proceeding on the singlet surface via a key diradical intermediate (**10a-Ph** or **10b-Ph**) or (2) concerted PhCCl addition−N_2 extrusion of the diazomethane isomer of **1a** or **1b** (**6a** or **6b**). The reactions in both cage systems are extremely exothermic, with energy releases of 86−96 kcal/mol

DOI: 10.1021/acs.joc.5b00456
J. Org. Chem. 2015, 80, 5049−5065

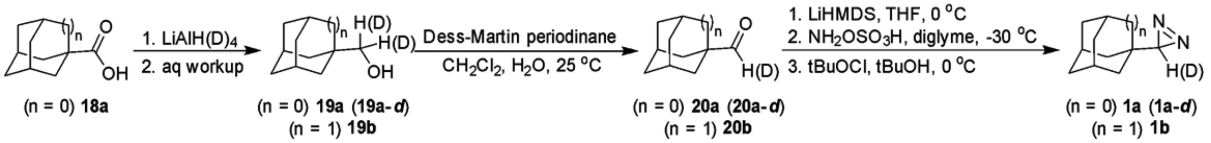

from the bridgehead alkenes + PhCCl. Preliminary direct dynamics trajectory calculations indicate the possible intervention of dynamic control of the adamantene−PhCCl system. Additional computational studies are thus underway on both systems.

EXPERIMENTAL SECTION

General. All reactions were performed under N_2 in oven-dried glassware unless otherwise noted. Anhydrous solvents were used as received. All other reagents were also used as received. NMR spectra were recorded in $CDCl_3$, cyclohexane-d_{12}, or benzene-d_6 at 300 MHz for ^{1}H spectra and 75 MHz for ^{13}C spectra. ^{1}H chemical shifts are reported in parts per million (δ) relative to tetramethylsilane (TMS, δ 0.00) using TMS as a reference. ^{13}C NMR chemical shifts are reported in parts per million; the center peak of the solvent signal is used as a reference. IR spectra were taken using an FT-IR spectrometer. IR absorptions are reported in cm^{-1}. Steady-state photolyses were conducted with a photochemical reactor at 300 or 350 nm. Laser flash photolysis experiments were conducted with an Nd:YAG laser at 355 nm. Details of the LFP system are provided in the Supporting Information. All quantitative product analyses were conducted with a gas chromatograph with a flame ionization detector using mesitylene as an internal standard. High-resolution mass spectra (HRMS) were recorded on a sector-type double-focusing instrument with electron ionization or fast-atom bombardment ionization.

Syntheses. Syntheses of noradamantyldiazirine (**1a**), noradamantyldiazirine-*d* (**1a-*d***), and adamantyldiazirine (**1b**) were conducted according to previously reported procedures by Platz and coworkers[18,19,29] and others.[45−48] Phenylchlorodiazirine was synthesized according to Graham's method.[30] Authentic samples of *E*- and *Z*-**4b-Ph** were synthesized according to a previous report.[49]

*Preparation of Noradamantyl Alcohol **19a** or **19a-d**.*[18,48] To an oven-dried, three-necked, 500-mL, round-bottom flask equipped with a reflux condenser, 125-mL addition funnel, magnetic stir bar, and glass stopper flushed with N_2 was cautiously and rapidly added $LiAlH(D)_4$ (1.85 g of $LiAlH_4$ (2.06 g of $LiAlD_4$), 49 mmol, 1.2 equiv). Anhydrous diethyl ether (85 mL) was added to dissolve the $LiAlH(D)_4$ via glass syringe. To an oven-dried, 100-mL, pear-shaped flask flushed with N_2 was added 3-noradamantylcarboxylic acid (**18a**) (6.77 g, 41 mmol, 1.0 equiv), which was dissolved in 82 mL of anhydrous tetrahydrofuran. The solution was then transferred to the addition funnel and added dropwise (∼1−2 drop/s) at room temperature to the stirring $LiAlH(D)_4$ solution. The reaction mixture was then refluxed for 2 h, cooled to room temperature, and further cooled in an ice bath. Ice-cold distilled water (2 mL) was added to the solution dropwise, followed by cold 15% aqueous NaOH solution (2 mL) and more distilled water (3 mL). The light gray precipitate was removed via vacuum filtration, rinsing with warm ether. The filtrate was dried over $MgSO_4$, filtered, concentrated by rotary evaporation, and dried under vacuum overnight. Crude noradamantyl alcohol [**19a**(-***d***)] was collected as an off-white solid and used without further purification. **19a**: 2.43 g, 39%; EI-MS (*m*/*z*) 152 (M+), 134, 121, 119, 105, 92, 79, 77, 67, 55, 41, 27; ^{1}H NMR (300 MHz, $CDCl_3$) δ 3.64 (s, 2 H), 2.19 (s, 2 H), 2.09 (m, 1 H), 1.65 (m, 11 H); ^{13}C NMR (75 MHz, $CDCl_3$) δ 69.3, 51.2, 46.1, 40.8, 44.2, 37.6, 35.7. **19a-*d***: 3.90 g, 63%; EI-MS (*m*/*z*) 154 (M+), 136, 125, 121, 107, 94, 79, 77, 67, 53, 39, 33, 25, 12; ^{1}H NMR (300 MHz, $CDCl_3$) δ 2.24 (s, 2 H), 2.13 (m, 1 H), 1.69 (m, 11 H); ^{13}C NMR (75 MHz, $CDCl_3$) δ 68.5, 51.0, 46.0, 44.2, 40.7, 37.6, 35.7; IR [ATR] (cm^{-1}) 3313, 2921, 2863, 2190, 2078.

*Preparation of Aldehydes **20a**, **20a-d**, or **20b**.*[18,19,47,48] To an oven-dried, 500-mL, three-neck, round-bottom flask equipped with a 125-mL addition funnel, two glass stoppers, and magnetic stir bar, all under an atmosphere of nitrogen, was added **19**a (1.56 g, 10 mmol, 1.0 equiv), **19a-*d*** (1.59 g, 10 mmol, 1.0 equiv), or **19b** (1.67 g, 10 mmol, 1.0 equiv), which was dissolved in 60 mL of anhydrous CH_2Cl_2. Dess−Martin periodinane (DMP) (6.53 g, 15 mmol, 1.5 equiv) was added to the solution and the mixture stirred. To a 250-mL, pear-shaped flask containing 100 mL of CH_2Cl_2 was added 400 μL of distilled H_2O via syringe. The wet CH_2Cl_2 mixture was mixed thoroughly and transferred by syringe to the reaction flask dropwise via addition funnel (∼1 drop/s). The cloudy white reaction mixture was stirred for 30 min and then diluted to 500 mL with ether. The mixture was concentrated by rotary evaporation to approximately 60 mL and diluted again with ether (to 100 mL). Excess unreacted DMP was removed by vacuum filtration. The reaction mixture was transferred to a 500 mL separatory funnel and washed with a 1:1 mixture of 10% $Na_2S_2O_3$ and saturated aqueous $NaHCO_3$ (80 mL, 40 mL of each solution), followed by H_2O (60 mL) and brine (60 mL). The aqueous layer was extracted with ether (80 mL), which was then washed with H_2O (40 mL) and brine (40 mL). The organic layers were combined, dried over $MgSO_4$, vacuum filtered, concentrated, and dried under vacuum, yielding an oily, pale yellow slush (**20a**) or granular, off-white crystals (**20a-*d*** and **20b**) that was used without further purification. **20a**: 0.91 g, 61%; ^{1}H NMR (300 MHz, $CDCl_3$) δ 9.74 (s, 1 H); ^{13}C NMR (75 MHz, $CDCl_3$) δ 205.5, 46.9, 43.8, 42.2, 37.6, 35.4, 34.8. **20a-*d***: 0.79 g, 52%; EI-MS (*m*/*z*) 151 (M+), 133, 121, 118, 109, 93, 79, 73, 67, 53, 39, 27, 15. **20b**: 1.56 g, 95%; EI-MS (*m*/*z*) 164 (M+), 145, 135, 119, 107, 93, 79, 67, 55, 41, 29, 25, 12.

*Preparation of Diazirines **1a**, **1a-d**, or **1b**.*[18,29,45] Crude aldehyde **20a** (0.91 g, 6.1 mmol, 1.0 equiv), **20a-*d*** (0.79 g, 5.2 mmol, 1.0 equiv), or **20b** (1.56 g, 9.5 mmol, 1.0 equiv) was dissolved in anhydrous THF (9−13 mL) in a pear-shaped flask. The solution was transferred via syringe to an oven-dried, three-necked, 250-mL, round-bottom flask, equipped with a low-temperature thermometer, two 25-mL addition funnels, and magnetic stir bar, all under N_2. The cloudy, orange-brown mixture was cooled to −5 °C using an acetone−dry ice bath. A 1.0 M solution of lithium bis(trimethylsilyl)amide in THF (17−20 mL, 17−20 mmol, 2.5 equiv) was added dropwise via addition funnel at 0 °C to form a transparent dark orange-brown mixture. The solution was stirred at 0 °C for 30 min and then cooled to −35 °C. Hydroxylamine-*O*-sulfonic acid (1.66−2.25 g, 17−20 mmol, 1.1 equiv) was dissolved in anhydrous diethylene glycol dimethyl ether (13−15 mL) in an oven-dried, 25-mL, pear-shaped flask under N_2 and added dropwise to the reaction vessel via addition funnel. The cloudy, yellow-orange mixture was warmed to 0 °C and stirred for 1 h over an ice−salt bath. The lights were dimmed and freshly prepared *tert*-butyl hypochlorite[45] (1.2 mL) in *tert*-butanol (1.4−1.7 mL) was added, behind a blast shield, dropwise via syringe after replacing one of the addition funnels with a rubber septum. The mixture was stirred for 30 min at 0 °C and distilled water (40 mL) was added. The reaction mixture was transferred to a 250 mL separatory funnel, extracted with pentane (2 × 20 mL), and then washed with distilled water (2 × 20 mL). The organic layer was transferred to an amber bottle, dried over magnesium sulfate, and stored at −80 °C. The diazirines were purified via column chromatography on silica gel (pentane eluent). **1a**: λ_{max} = 337, 344, 355 nm; ^{1}H NMR (300 MHz, C_6D_6) δ 2.09 (t, J = 6.4 Hz, 1H), 1.92 (br s, 2H), 1.48−1.19 (m, 10H), 0.51 (s, 1H); ^{13}C NMR (75 MHz, C_6D_6) δ 48.4, 46.5, 44.3, 41.9, 37.6, 35.3, 27.0, 2.4. **1a-*d***: λ_{max} = 337, 344, 354 nm; ^{1}H NMR (300 MHz, $CDCl_3$) δ 2.26 (t, J = 6.6 Hz, 1H), 2.20 (br s, 2H), 1.58−1.43 (m, 10H); ^{13}C NMR (75 MHz, $CDCl_3$) δ 48.0, 46.3, 44.1, 41.6, 37.3, 35.2. **1b**: λ_{max} = 337, 344, 355 nm; ^{1}H NMR (300 MHz, $CDCl_3$) δ 1.89 (br s, 2 H), 1.64−1.51 (m, 6H), 1.32 (d, J = 2.7 Hz, 6H); ^{13}C NMR (75 MHz, $CDCl_3$) δ 39.5, 36.8, 31.8, 29.7, 28.2.

*Phenylchlorodiazirine (**8**).*[30] To a mixture of lithium chloride (3.57 g, 84 mmol, 12 equiv) and benzamidine hydrochloride (1.09 g, 7.0 mmol, 1.0 equiv) were added 50 mL of dimethyl sulfoxide and 50 mL

DOI: 10.1021/acs.joc.5b00456
J. Org. Chem. 2015, 80, 5049−5065

of pentane in a three-neck, 1-L, round-bottom flask fitted with a 125-mL addition funnel, large stir bar, and thermometer. Aqueous NaOCl solution (100 mL, 8.25% hypochlorite) saturated with sodium chloride was added slowly, the temperature being maintained between 35 and 40 °C with an ice bath. After 5 min, 88 mL of DMSO, 25 mL of pentane, and 150 mL of aqueous NaOCl were added, and the mixture was allowed to stir for 1 h at room temperature. The reaction solution was poured into a separatory funnel containing 300 mL of ice water, and the pentane layer was separated, washed with brine (4 × 250 mL), and dried over $CaCl_2$. The crude diazirine **8** was chromatographed on a silica gel column with pentane eluent, affording pure **8**: λ_{max} = 390, 385, 379, 369, 351; ^{1}H NMR (300 MHz, $CDCl_3$) δ 7.39 (m, 3 H), 7.11 (m, 2 H); ^{13}C NMR (75 MHz, $CDCl_3$) δ 135.9, 129.5, 128.7, 126.2.

*E- and Z-2-Adamantyl-1-chloro-1-phenylethene (**4b-Ph**).*[49] To an oven-dried, 25-mL, round-bottom flask under an atmosphere of N_2 and equipped with a magnetic stir bar were added 1-chloroadamantane (720 mg, 4.2 mmol), 1-phenyl-2-trimethylsilylacetylene (700 mg, 4 mmol), and zinc chloride (1.8 g, 14 mmol) in anyhydrous CH_2Cl_2 (8 mL). This mixture was kept under nitrogen and stirred for 48 h at room temperature. Color changes were observed over the 48-h stirring period: the mixture turned from white to off-white to yellow to light green to dark green. The crude, thick, dark green reaction mixture containing **4b-Ph** (0.71 g, 72%) was collected, concentrated by rotary evaporation, and dried under vacuum. The *E*- and *Z*-isomers of **4b-Ph** were separated and purified by column chromatography (pentane eluent). The identity of these compounds in the photolysis mixture of adamantyldiazirine (**1b**) and phenylchlorodiazirine (**8**) was confirmed by a GC spiking experiment: the photolysis mixture was spiked with authentic *E*- and *Z*-**4b-Ph**. Characterization data follow below.

*E-2-Adamantyl-1-chloro-1-phenylethene (**E-4b-Ph**).* mp 75−77 °C (lit.[49] mp 74−75 °C); ^{1}H NMR (300 MHz, $CDCl_3$) δ 7.25 (s, 5H), 5.72 (s, 1H), 1.76 (m, 3H), 1.48 (m, 12H); ^{13}C NMR (75 MHz, $CDCl_3$) δ 140.6, 139.6, 129.7, 129.3, 128.5, 42.9, 36.8, 36.6, 28.5; GC/MS (EI) (t_R = 11.7 min) *m*/*z* (rel intensity) 272/274 [83.3/26.7, $M^+/(M^+ + 2)$], 237 (100, $M^+ - 35$), 179 (71.1, $M^+ - 93$), 141 (51.1, $M^+ - 131$), 115 (22.2, $M^+ - 157$), 91 (17.8, $M^+ - 181$), 79 (15.6, $M^+ - 193$); HRMS (FAB+) calcd for $C_{18}H_{21}Cl$ 272.1332, found 272.1326.

*Z-2-Adamantyl-1-chloro-1-phenylethene (**Z-4b-Ph**).* ^{1}H NMR (300 MHz, $CDCl_3$) δ 7.45 (dd, *J* = 1.7, 8.1 Hz, 2H), 7.24 (m, 3H), 5.79 (s, 1H), 1.94 (br s, 9H), 1.67 (br s, 6H); ^{13}C NMR (75 MHz, $CDCl_3$) δ 140.3, 137.4, 130.3, 128.12, 128.06, 126.6, 41.1, 36.8, 35.7, 28.6; GC/MS (EI) (t_R = 12.3 min) *m*/*z* (rel intensity) 272/274 [100/33.8, $M^+/(M^+ + 2)$], 237 (100, $M^+ - 35$), 179 (81.2, $M^+ - 93$), 141 (57.5, $M^+ - 131$), 128 (18.8, $M^+ - 144$), 115 (25.0, $M^+ - 157$), 91 (25.0, $M^+ - 181$), 79 (20.0, $M^+ - 193$); HRMS (FAB+) calcd for $C_{18}H_{21}Cl$ 272.1332, found 272.1339.

Steady State Photolyses—Quantitative Product Studies. Stock solutions in pentane of each of the diazirines **1a**, **1a-*d***, and **1b** were prepared to concentrations of A_{355} = 2.6 {[**1a**] = [**1a-*d***] = 7.9 mM (ε = 330 M^{-1} cm^{-1}); [**1b**] = 6.0 mM (ε = 430 M^{-1} cm^{-1})}. A stock solution in pentane of phenylchlorodiazirine (**8**) was prepared to a concentration of $A_{389} \approx 3$ {[**8**] = 30 mM (ε = 100 M^{-1} cm^{-1})}. A stock solution of diazirine **1a** in pentane or **1b** in pentane was combined with a stock solution of **8** in pentane in a quartz cuvette to a total volume of 1.5 mL. The resulting prephotolysis diazirine absorptions were as follows: **1a** and **1a-*d***, A_{355} = 0.9−1.0; **1b**, A_{350} = 0.7−0.9; **8**, A_{390} = 0.7−1.2. Three cuvettes each of **1a** + **8**, **1a-*d*** + **8**, and **1b** + **8** were prepared. Then, each of the six cuvettes was purged with N_2 for approximately 1 min and subsequently irradiated at 350 nm for 1−2 h at room temperature, monitoring the photolysis by UV−vis. After all of the diazirines were consumed, 1.5 μmol of mesitylene [10 μL of 0.15 M mesitylene (in pentane solvent)] was added as an internal standard to each cuvette. Each sample was analyzed by GC/FID in triplicate. Results are reported in the Supporting Information.

Isolation of Ethylenes 4a-Cl and *E*- and *Z*-4a-Ph. Ethylenes **4a-Cl** and *E*- and *Z*-**4a-Ph** were isolated from steady-state photolysis mixtures via column chromatography on silica gel (pentane eluent). Several successive columns were required for complete separation and purification of these products, especially for the separation of *E*- and *Z*-**4a-Ph**.

*1,1-Dichloro-2-noradamantylethene (**4a-Cl**).* ^{1}H NMR (300 MHz, $CDCl_3$) δ 6.14 (s, 1H), 2.50 (t, *J* = 6.7 Hz, 1H), 2.24 (s, 2H), 1.88−1.84 (m, 6H), 2.55−1.62 (m, 4H); ^{13}C NMR (75 MHz, $CDCl_3$) δ 138.0, 49.6, 49.2, 45.1, 43.9, 37.6, 35.0; GC/MS (EI) (t_R = 9.9 min) *m*/*z* (rel intensity) 216/218/220 [13.0/9.3/3.7, $M^+/(M^+ + 2)/(M^+ + 4)$], 181/183 [12.0/3.8, $(M^+ - 35)/((M^+ + 2) - 35)$], 173 (11.1, $M^+ - 43$), 145 (7.4, $M^+ - 71$), 139 (8.1, $M^+ - 77$), 125 (7.7, $M^+ - 91$), 103 (11.1, $M^+ - 113$), 91 (29.6, $M^+ - 125$), 80 (100, $M^+ - 81$), 51 (16.7, $M^+ - 165$); HRMS (EI+) calcd for $C_{11}H_{14}Cl_2$ 216.0473, found 216.0466.

*E-1-Chloro-2-noradamantyl-1-phenylethene (**E-4a-Ph**).* ^{1}H NMR (300 MHz, $CDCl_3$) δ 7.40−7.30 (m, 5H), 6.28 (s, 1H), 2.21 (t, *J* = 6.7 Hz, 1H), 2.08 (s, 2H), 1.70−1.35 (m, 14H); ^{13}C NMR (75 MHz, $CDCl_3$) δ 139.3, 138.6, 129.8, 129.5, 128.6, 128.2, 50.3, 46.9, 43.8, 37.8, 34.8, 34.3; GC/MS (EI) (t_R = 12.3 min) *m*/*z* (rel intensity) 258 (3.7, M^+), 223 (100, $M^+ - 35$), 179/181 [32.4/14.8, $(M^+ - 79)/((M^+ + 2) - 79)$], 152 (23.1, $M^+ - 106$), 143 (70.4, $M^+ - 115$), 115 (40.7, $M^+ - 143$), 103 (15.0, $M^+ - 155$), 91 (41.7, $M^+ - 167$), 79 (59.3, $M^+ - 179$), 65 (18.5, $M^+ - 193$); HRMS (EI+) calcd for $C_{17}H_{19}Cl$ 258.1175, found 258.1169.

*Z-1-Chloro-2-noradamantyl-1-phenylethene (**Z-4a-Ph**).* ^{1}H NMR (300 MHz, $CDCl_3$) δ 7.59 (m, 2H), 7.34 (m, 3H), 6.39 (s, 1H), 2.65 (t, *J* = 6.7 Hz, 1H), 2.28 (s, 2H), 2.07−1.92 (m, 6H), 1.69−1.54 (m, 5H); ^{13}C NMR (75 MHz, $CDCl_3$) δ 139.6, 136.2, 131.6, 128.4, 128.3, 126.5, 49.8, 49.6, 45.2, 44.0, 37.8, 35.3; GC/MS (EI) (t_R = 12.3 min) *m*/*z* (rel intensity) 258/260 [(11.0/3.7, $M^+/(M^+ + 2)$), 223 (100, $M^+ - 35$), 179/181 [28.0/9.8, $(M^+ - 79)/((M^+ + 2) - 79)$], 165, (29.3, $M^+ - 93$), 152 (15.9, $M^+ - 106$), 143 (65.9, $M^+ - 115$), 115 (34.1, $M^+ - 143$), 91 (37.8, $M^+ - 167$), 79 (54.9, $M^+ - 179$), 65 (14.6, $M^+ - 193$); HRMS (EI+) calcd for $C_{17}H_{19}Cl$ 258.1175, found 258.1172.

Laser Flash Photolysis (LFP) Studies. Stock solutions in pentane of the diazirines **1a**, **1a-*d***, and **1b** were prepared to a concentration of A_{355} = 2.6 ([**1a**] = [**1a-*d***] = 7.9 mM; [**1b**] = 6.0 mM). A stock solution in pentane of phenylchlorodiazirine (**8**) was prepared to a concentration of $A_{389} \approx 3$ ([**8**] = 30 mM). For the measurements of **1a** + **8**, a stock solution of anhydrous pyridine in pentane was also prepared at a concentration of 2 mM. For the noradamantylcarbene/adamantene studies, into duplicate quartz LFP cuvettes were placed 100, 200, 300, 400, or 500 μL of the **1a** (or **1a-*d***) stock solution; 250 μL of the **8** stock solution; 10 μL of the pyridine stock solution; and the remainder (740−1140 μL) of pentane for a total volume of 1500 μL. Thus, the final (LFP) concentrations were [**1a**] = [**1a-*d***] = 0.525−2.6 mM, [**8**] = 5 mM, [pyridine] = 0.013 mM. For the adamantylcarbene/homoadamantene system, into duplicate quartz LFP cuvettes were placed 450 μL of **1b**, 200 μL of **8**, and 850 μL of pentane for a total volume of 1500 μL. Thus, the final (LFP) concentrations were [**1b**] = 1.8 mM and [**8**] = 4 mM. Each LFP cuvette was capped with a rubber septum and purged with argon for 45−60 s. For the LFP measurements, each cuvette was subjected to three sets of five laser pulses at 355 nm (Nd:YAG), where the signal outputs for each set of pulses were averaged. For **1a** (or **1a-*d***) + **8** + pyridine, we monitored the growth of the PhCCl−pyridine ylide at 480 nm. For **1b** + **8**, we monitored the decay of PhCCl at 320 nm. Rate constant data from LFP measurements appear in the Supporting Information.

■ COMPUTATIONAL METHODS

All calculations were performed with Gaussian 09[35] in the gas phase. Molecular geometries were optimized using UB3LYP/6-31+G(d,p)[50,51] and single-point energies were calculated at UM062X/6-31+G(d,p).[52,53] Stationary points were verified by the existence of no imaginary frequencies for energy minima and exactly one imaginary frequency for transition-state structures. All energies reported are electronic energies without zero-point corrections or Gibbs free energies, unless otherwise noted. Three-dimensional molecular images were generated with CylView.[54] Direct dynamics trajectories were initiated at **3a** + PhCCl *TS 2* using Progdyn,[55] which utilizes Gaussian

DOI: 10.1021/acs.joc.5b00456
J. Org. Chem. 2015, 80, 5049−5065

09 to calculate force constants. Trajectories were run at the UB3LYP/6-31+G(d,p) level of theory with a time step of 1 fs. Stopping parameters for the trajectories were defined as follows: a trajectory was considered to produce separated reactants when the C2−C11 distance was greater than 5 Å (atom numbers shown below). A trajectory formed cyclopentene **14a-Ph** when the C1−C12 distance was less than 1.62 Å, which is within 4% of the C1−C12 distance in its ground-state, optimized structure (1.56 Å). Cyclopropane **9a-Ph** was formed when the C1−C11 distance was less than 1.58 Å, also within 4% of the same distance in its optimized structure (1.53 Å). A more rigid stopping criterion for **4a-Ph** was imposed, in which the C1−C3 distance had to be less than 1.59 Å to say with confidence that the noradamantyl moiety had been formed (where the C1−C3 distance in the optimized structure of **4a-Ph** was 1.61 Å).

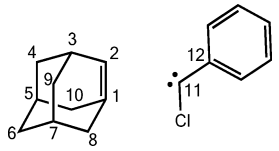

■ ASSOCIATED CONTENT

Supporting Information

NMR spectra of **4a-Cl**, *E*- and *Z*-**4a-Ph**, and *E*- and *Z*-**4b-Ph**; product study results; data from the NMR kinetic studies; details of the LFP system; and computational details including IRC data, Cartesian coordinates, and imaginary frequencies of all stationary points. The Supporting Information is available free of charge on the ACS Publications website at DOI: 10.1021/acs.joc.5b00456.

■ AUTHOR INFORMATION

Corresponding Author

*E-mail: dmerrer@barnard.edu

Notes

The authors declare no competing financial interest.

■ ACKNOWLEDGMENTS

We are grateful to the Thamattoor group for providing us with phenanthride **7** and for being helpful hosts during our trips to Colby College for the LFP studies. We also thank Profs. Wes Borden, Kathleen Morgan, Paul Rablen, and Christian Rojas for helpful discussions. We thank Drs. John Decatur and Yasuhiro Itagaki of Columbia University for NMR and HRMS assistance, respectively. D.J.T. and S.R.H. thank the National Science Foundation's XSEDE program (CHE-030089) and the U.S. Department of Education's GAANN Fellowship for support. D.C.M. acknowledges the NSF (CHE-0844034), ACS-PRF (52099-UR4), Con Edison (F.D.), the Howard Hughes Medical Institute (E.D., J.C.T.), the Jewish Foundation for Education of Women (M.O.), and Barnard College for financial support.

■ REFERENCES

(1) Hoffmann, R.; Hopf, H. *Angew. Chem., Int. Ed.* **2008**, *47*, 4474−4481.
(2) Bredt, J. *Justus Liebigs Ann. Chem.* **1924**, *437*, 1−13.
(3) Warner, P. M. *Chem. Rev.* **1989**, *89*, 1067−1093.
(4) Novak, I. *J. Chem. Inf. Model.* **2005**, *45*, 334−338.
(5) Mak, J. Y. W.; Pouwer, R. H.; Williams, C. M. *Angew. Chem., Int. Ed.* **2014**, *53*, 13664−13688.
(6) Nguyen, Q. N. N.; Tantillo Dean, J. *Beilstein J. Org. Chem.* **2013**, *9*, 323−331.
(7) Martella, D. J.; Jones, M., Jr.; Schleyer, P. v. R. *J. Am. Chem. Soc.* **1978**, *100*, 2896−2897.
(8) Conlin, R. T.; Miller, R. D.; Michl, J. *J. Am. Chem. Soc.* **1979**, *101*, 7637−7638.
(9) Bian, N.; Jones, M., Jr. *J. Am. Chem. Soc.* **1995**, *117*, 8957−8961.
(10) Jones, M., Jr. In *Advances in Carbene Chemistry*; Brinker, U. H., Ed.; JAI Press: Stamford, CT, 1998; Vol. *2*, p 77−96.
(11) Martella, D. J.; Jones, M., Jr.; Schleyer, P. v. R.; Maier, W. F. *J. Am. Chem. Soc.* **1979**, *101*, 7634−7637.
(12) Ruck, R. T.; Jones, M., Jr. *Tetrahedron Lett.* **1998**, *39*, 4433−4436.
(13) Wolf, A. D.; Jones, M., Jr. *J. Am. Chem. Soc.* **1973**, *95*, 8209.
(14) Farcasiu, M.; Farcasiu, D.; Conlin, R. T.; Jones, M., Jr.; Schleyer, P. v. R. *J. Am. Chem. Soc.* **1973**, *95*, 8207.
(15) Michl, J.; Radziszewski, G. J.; Downing, J. W.; Kopecky, J.; Kaszynski, P.; Miller, R. D. *Pure Appl. Chem.* **1987**, *59*, 1613−1626.
(16) Michl, J.; Radziszewski, G. J.; Downing, J. W.; Wiberg, K. B.; Walker, F. H.; Miller, R. D.; Kovacic, P.; Jawdosiuk, M.; Bonacic-Koutecky, V. *Pure Appl. Chem.* **1983**, *55*, 315−321.
(17) Geise, C. M.; Hadad, C. M. *J. Am. Chem. Soc.* **2000**, *122*, 5861−5865.
(18) Tae, E. L.; Ventre, C.; Zhu, Z.; Likhotvorik, I.; Ford, F.; Tippmann, E.; Platz, M. S. *J. Phys. Chem. A* **2001**, *105*, 10146−10154.
(19) Tae, E. L.; Zhu, Z.; Platz, M. S. *J. Phys. Chem. A* **2001**, *105*, 3803−3807.
(20) Jackson, J. E.; Soundararajan, N.; Platz, M. S.; Liu, M. T. H. *J. Am. Chem. Soc.* **1988**, *110*, 5595−5596.
(21) Jackson, J. E.; Platz, M. S. In *Advances in Carbene Chemistry*; Brinker, U. H., Ed.; JAI Press: Stamford, CT, 1994; Vol. *1*, p 89−160.
(22) Weber, J.; Brinker, U. H. *Angew. Chem., Int. Ed. Engl.* **1997**, *36*, 1623−1626.
(23) Weber, J.; Xu, L.; Brinker, U. H. *Tetrahedron Lett.* **1992**, *33*, 4537−4540.
(24) Khrapunovich, M.; Zelenova, E.; Seu, L.; Sabo, A. N.; Flaherty, A.; Merrer, D. C. *J. Org. Chem.* **2007**, *72*, 7574−7580.
(25) Merrer, D. C.; Rablen, P. R. *J. Org. Chem.* **2005**, *70*, 1630−1635.
(26) Merrer, D. C.; Doubleday, C. *J. Phys. Org. Chem.* **2011**, *24*, 947−951.
(27) Rablen, P. R.; Paiz, A. A.; Thuronyi, B. W.; Jones, M. *J. Org. Chem.* **2009**, *74*, 4252−4261.
(28) Anslyn, E. V.; Dougherty, D. A. *Modern Physical Organic Chemistry*; University Science: Sausalito, CA, 2006.
(29) Likhotvorik, I. R.; Tae, E. L.; Ventre, C.; Platz, M. S. *Tetrahedron Lett.* **2000**, *41*, 795−796.
(30) Graham, W. H. *J. Am. Chem. Soc.* **1965**, *87*, 4396.
(31) Chateauneuf, J. E.; Johnson, R. P.; Kirchhoff, M. M. *J. Am. Chem. Soc.* **1990**, *112*, 3217−3218.
(32) Joshi, G. C.; Singh, N.; Pande, L. M. *Synthesis* **1972**, 317.
(33) Robert, M.; Likhotvorik, I.; Platz, M. S.; Abbot, S. C.; Johnson, R. P. *J. Phys. Chem. A* **1998**, *102*, 1507−1513.
(34) Becker, K. B. *Helv. Chim. Acta* **1977**, *60*, 81−93.
(35) Frisch, M. J.; Trucks, G. W.; Schlegel, H. B.; Scuseria, G. E.; Robb, M. A.; Cheeseman, J. R.; Scalmani, G.; Barone, V.; Mennucci, B.; Petersson, G. A.; Nakatsuji, H.; Caricato, M.; Li, X.; Hratchian, H. P.; Izmaylov, A. F.; Bloino, J.; Zheng, G.; Sonnenberg, J. L.; Hada, M.; Ehara, M.; Toyota, K.; Fukuda, R.; Hasegawa, J.; Ishida, M.; Nakajima, T.; Honda, Y.; Kitao, O.; Nakai, H.; Vreven, T.; Montgomery, J. J. A.; Peralta, J. E.; Ogliaro, F.; Bearpark, M.; Heyd, J. J.; Brothers, E.; Kudin, K. N.; Staroverov, V. N.; Kobayashi, R.; Normand, J.; Raghavachari, K.; Rendell, A.; Burant, J. C.; Iyengar, S. S.; Tomasi, J.; Cossi, M.; Rega, N.; Millam, N. J.; Klene, M.; Knox, J. E.; Cross, J. B.; Bakken, V.; Adamo, C.; Jaramillo, J.; Gomperts, R.; Stratmann, R. E.; Yazyev, O.; Austin, A. J.; Cammi, R.; Pomelli, C.; Ochterski, J. W.; Martin, R. L.; Morokuma, K.; Zakrzewski, V. G.; Voth, G. A.; Salvador, P.; Dannenberg, J. J.; Dapprich, S.; Daniels, A. D.; Farkas, Ö.; Foresman, J. B.; Ortiz, J. V.; Cioslowski, J.; Fox, D. J. *Gaussian 09*, Revision A.01; Gaussian, Inc.: Wallingford, CT, 2009.
(36) Pliego, J. R.; De Almeida, W. B.; Celebi, S.; Zhu, Z.; Platz, M. S. *J. Phys. Chem. A* **1999**, *103*, 7481−7486.

DOI: 10.1021/acs.joc.5b00456
J. Org. Chem. 2015, 80, 5049−5065

(37) Scott, A. P.; Platz, M. S.; Radom, L. *J. Am. Chem. Soc.* **2001**, *123*, 6069.
(38) Ess, D. H.; Houk, K. N. *J. Am. Chem. Soc.* **2007**, *129*, 10646−10647.
(39) Ess, D. H.; Houk, K. N. *J. Am. Chem. Soc.* **2008**, *130*, 10187−10198.
(40) Merrer, D. C.; Houk, K. N.; Xu, L. In *Contemporary Carbene Chemistry*; Moss, R. A., Doyle, M. P., Eds.; Wiley: Hoboken, NJ, 2013; p 131−165.
(41) Mo, X. Y.; Bernard, S. E.; Khrapunovich, M.; Merrer, D. C. *J. Org. Chem.* **2008**, *73*, 8537−8544.
(42) Carpenter, B. K. *Acc. Chem. Res.* **1992**, *25*, 520−528.
(43) Carpenter, B. K. *J. Phys. Org. Chem.* **2003**, *16*, 858−868.
(44) Carpenter, B. K. *Annu. Rev. Phys. Chem.* **2005**, *56*, 57−89.
(45) Mintz, M. J.; Walling, C. *Org. Synth.* **1969**, *49*, 9−12.
(46) Farooq, O.; Marcelli, M.; Prakash, G. K. S.; Olah, G. A. *J. Am. Chem. Soc.* **1988**, *110*, 864−867.
(47) Meyer, S. D.; Schreiber, S. L. *J. Org. Chem.* **1994**, *59*, 7549−7552.
(48) Vogt, B. R.; Hoover, J. R. E. *Tetrahedron Lett.* **1967**, *8*, 2841−2843.
(49) Ohno, M.; Sasaki, T.; Usuki, A. *J. Org. Chem.* **1980**, *45*, 3559−3564.
(50) Becke, A. D. *J. Chem. Phys.* **1993**, *98*, 5648.
(51) Becke, A. D. *J. Chem. Phys.* **1993**, *98*, 1372−1377.
(52) Zhao, Y.; Truhlar, D. G. *Acc. Chem. Res.* **2008**, *41*, 157−167.
(53) Zhao, Y.; Truhlar, D. G. *Theor. Chem. Acc.* **2008**, *120*, 215−241.
(54) Legault, C. Y. *CYLview*, version 1.0b, Université de Sherbrooke, 2009.
(55) Ussing, B. R.; Hang, C.; Singleton, D. A. *J. Am. Chem. Soc.* **2006**, *128*, 7594−7607.

DOI: 10.1021/acs.joc.5b00456
J. Org. Chem. 2015, 80, 5049−5065